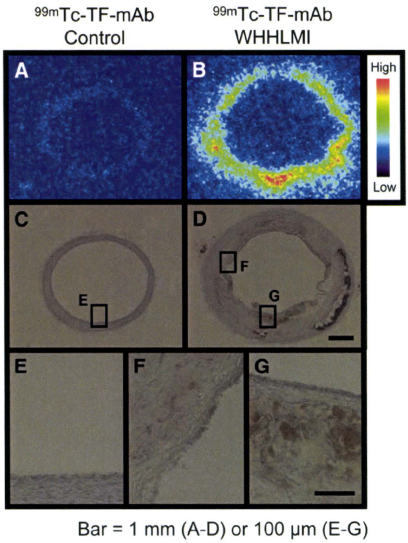

FIGURE 5. Regional distribution of ^{99m}Tc-TF-mAb and TF expression in aortic sections. Autoradiogram (A and B) and TF immunohistochemical staining (C–G) of control (C and E) and WHHLMI rabbits (D, F, and G). (E–G) High-magnification images of TF immunohistochemical staining in regions depicted in C and D. Identical color window was applied to both autoradiographic images (A and B). Bar = 1 mm (A–D) and 100 μm (E–G).

index were both observed in atheromatous lesions. In contrast, ^{99m}Tc-IgG$_1$ accumulation in lesions was low and did not correlate with the histologic grade of lesions, with no significant differences among the lesion types (Fig. 4B).

DISCUSSION

In the present study, we designed a new imaging agent, ^{99m}Tc-TF-mAb, for the purpose of discriminating atherosclerotic lesions at higher risk for rupture (thrombogenic atheromatous lesions) from more stable lesions and evaluated the potential of ^{99m}Tc-TF-mAb using an atherosclerotic rabbit model. Our major findings are that a positive correlation was demonstrated between regional ^{99m}Tc-TF-mAb accumulation and TF expression density in atherosclerotic lesions of WHHLMI rabbits but not with ^{99m}Tc-IgG$_1$ and that significantly higher ^{99m}Tc-TF-mAb accumulation was found in grade IV, more vulnerable atheromatous lesions, than in neointimal lesions or other more stable lesions. Thus, we demonstrate the potential of ^{99m}Tc-TF-mAb for molecular imaging of TF expression and selectively detecting atheromatous plaques at higher risk for rupture.

Immunoreactivity and Specificity of ^{99m}Tc-TF-mAb

Immunoreactivity, specificity, and detectable but functionally silent labeling are indispensable prerequisites of in vivo molecular imaging probes using immunodetection. In this study, flow cytometric analyses indicated that modification of TF-mAb with HYNIC did not significantly affect the immunoreactivity of the original TF-mAb. In addition, autoradiography and immunohistochemical studies showed that ^{99m}Tc-TF-mAb accumulation in atherosclerotic lesions correlated well with TF expression density, which was higher in atheromatous lesions, as expected (Figs. 3A and 4A). Further, contrary to the results with ^{99m}Tc-TF-mAb (Fig. 4A), the results with ^{99m}Tc-IgG$_1$ (Fig. 4B) showed that accumulation of ^{99m}Tc-labeled nonspecific IgG in atheromatous lesions was not significantly different from that in other types of lesions (i.e., neointimal, fibroatheromatous, and collagen-rich lesions). These findings strongly suggest the potential of ^{99m}Tc-TF-mAb to specifically recognize TF in vivo.

TF as a Target Molecule for Plaque Imaging

TF, selected as a target molecule for molecular imaging in this study, initiates the exogenous blood coagulation cascade leading to thrombus formation in vivo and represents a good marker for late-stage vulnerable lesions. TF in atherosclerotic lesions was identified in several cell types, such as endothelial cells, smooth muscle cells, monocytes, macrophages, and foam cells (*3*), similar to lectinlike oxidized low-density lipoprotein receptor 1 (LOX-1). TF expression is reported to be increased in the later stages of atheromatous progression and thus was selectively detected in atheromatous lesions in this report (Fig. 4). These findings are comparable to those of our previous immunohistochemical study (*5*) and another human study (*4*). On these bases, TF should be a potential target for detecting atheromatous plaques at higher risk for rupture in vivo. To our knowledge, this is the first report of the development of an in vivo TF imaging probe.

On the other hand, a series of imaging agents has targeted fibrin and factor XIII in thrombi using antibodies or peptides (*1*), with at least partial success. In the blood-coagulation cascade, TF initiates the system, and factor XIII covalently cross-links fibrin polymers and renders the thrombus more resistant to lysis. Therefore, ^{99m}Tc-TF-mAb will be useful for the early detection of the cascade, and fibrin and factor XIII imaging probes can detect later stages and thrombi themselves. In this study, ^{99m}Tc-TF-mAb corresponded with TF expression and showed preferential accumulation in atheromatous lesions and in lesions with increased vulnerability. Although further studies are required to investigate which target molecules in the cascade are most appropriate to estimate how unstable or vulnerable a plaque is in vivo, TF is a potential target. Furthermore, because great efforts have been made in the development of anticoagulation and antiplatelet pharmaceuticals for the treatment of atherosclerosis and

hyperlipidemia, effective imaging probes to target blood-coagulation cascades are also required for efficient drug development.

Limitations of ^{99m}Tc-TF-mAb

One drawback of ^{99m}Tc-TF-mAb is its relatively slow clearance from the blood, which is an intrinsic problem of molecular probes using antibodies. Recent advances in antibody engineering, however, should provide a promising solution for this issue. Radioprobes derived from low-molecular-weight polypeptides or compounds, small recombinant antibody fragments (Fab, scFv), engineered variants (diabodies, triabodies, minibodies, and single-domain antibodies), or pretargeting antibody methods show rapid clearance of radioactivity from the circulation (*19–21*). Image-subtraction techniques (*22–24*) or kinetic model analysis (*25,26*) may also help solve this issue. Accordingly, ^{99m}Tc-TF-mAb or its derivatives have great potential as in vivo molecular imaging probes and deserve further investigation.

A higher renal accumulation of ^{99m}Tc-IgG$_1$ than of ^{99m}Tc-TF-mAb was observed in WHHLMI rabbits. Although an exact mechanistic explanation for this significant difference is not clear, several other investigators have also reported a relatively high renal accumulation after the injection of radiolabeled mAbs (*27–29*). Because we evaluated the biodistribution 24 h after the injection (relatively late phase), renal accumulation may be ascribed to metabolic or degradation products of ^{99m}Tc-labeled antibodies (*30*). Thus, further ex vivo metabolite analysis studies could help to clarify the mechanism. In addition, it is known that the excretion system of WHHLMI rabbits is compromised (*31*), which could alter the renal accumulation of tracers. On the other hand, although a certain degree of TF expression was observed in glomeruli (*32*), this could not be a reason for the higher renal accumulation of ^{99m}Tc-IgG$_1$.

Recently, the focus of anticoagulant research has turned to inhibition of the TF-FVIIa complex, and many pharmaceutical industry research programs have attempted to discover TF-FVIIa complex inhibitors (*33*). Studies in monkeys have indicated that inhibition of the TF-FVIIa complex, compared with other anticoagulants that inhibit thrombin or FXa, results in an improved profile . It is well known that the pathways for blood coagulation are interdependent, and the initiation, amplification, and propagation stages are closely regulated by positive and negative feedback loops. Thus, repeated doses of anticoagulants might increase the expression of ineffective (silent) TF complex in plaques because of such feedback processes independent of the antiatherosclerotic effect, although a lowering of net TF expression would be expected. The TF antibody we established in this study recognizes 193Ser-207Cys in the extracellular domain, which is distant from the protein sites related to complex formation with FVIIa. Therefore, the ^{99m}Tc-TF-mAb we developed can estimate the net TF expression in plaques, providing a useful tool to investigate the effect of such anticoagulants in vivo.

Comparison with Other Imaging Probes

In the search for suitable molecular probes to assess atherosclerotic lesion characteristics, many targets, including macrophage activity, angiogenesis, apoptosis, and cell tracking (monocyte, stem cell, lymphocyte), have been assessed (*1,2,34–36*). However, the usefulness of these probes is still under preliminary investigation, except for ^{18}F-FDG, a marker of inflammation, and ^{99m}Tc-annexin A5, a marker of ongoing apoptotic cell death, which are currently in clinical studies. In previous studies, we evaluated macrophage imaging using ^{18}F-FDG (*11*) and also ^{99m}Tc-LOX-1-mAb (*17*), which targets a scavenger receptor highly expressed on macrophages and foam cells and showed the usefulness for detection of atherosclerotic lesions. However, ^{18}F-FDG accumulated in relatively stable lesions because of the presence of macrophages in such lesions, as also seen in this report (Fig. 4). We also previously showed a certain degree of LOX-1 expression in relatively stable lesions with ^{99m}Tc-LOX-1-mAb. As for ^{99m}Tc-annexin A5, the accumulation ratios of atheromatous lesions to other lesions of ^{99m}Tc-TF-mAb (atheromatous to neointimal, 3.0; atheromatous to fibroatheromatous, 2.4; and atheromatous to collagen-rich, 2.9) were markedly higher than those of ^{99m}Tc-annexin A5 (atheromatous to neointimal,1.3; atheromatous to fibroatheromatous, 1.3; atheromatous to collagen-rich, 1.8) (*15*). Our previous study in apolipoprotein E–null mice also showed relatively high ^{18}F-FDG accumulation levels in early lesions, resulting in lower accumulation ratios for advanced to early lesions in comparison with ^{99m}Tc-annexin A5 (*37*). Thus, the desirable features of ^{99m}Tc-TF-mAb further confirm its potential as a molecular probe for detecting atheromatous lesions at higher risk for rupture.

CONCLUSION

In this study, we succeeded in determining TF expression using ^{99m}Tc-TF-mAb in WHHLMI rabbits. Consequently, we demonstrated prominently higher accumulation of ^{99m}Tc-TF-mAb in grade IV atheroma. These findings strongly indicate that molecular imaging of TF should provide clinically useful information on the thrombogenicity of atherosclerotic plaques.

ACKNOWLEDGMENTS

This work was partly supported by a grant-in-aid for general scientific research from the Ministry of Education, Culture, Sports, Science and Technology of Japan and from the Japan Society for the Promotion of Science and by a research grant from the Association for Nuclear Technology in Medicine and Takeda Science Foundation.

REFERENCES

1. Shaw SY. Molecular imaging in cardiovascular disease: targets and opportunities. *Nat Rev Cardiol.* 2009;6:569–579.
2. Saraste A, Nekolla SG, Schwaiger M. Cardiovascular molecular imaging: an overview. *Cardiovasc Res.* 2009;83:643–652.

3. Moons AH, Levi M, Peters RJ. Tissue factor and coronary artery disease. *Cardiovasc Res.* 2002;53:313–325.
4. Jeanpierre E, Le Tourneau T, Six I, et al. Dietary lipid lowering modifies plaque phenotype in rabbit atheroma after angioplasty: a potential role of tissue factor. *Circulation.* 2003;108:1740–1745.
5. Kuge Y, Kume N, Ishino S, et al. Prominent lectin-like oxidized low density lipoprotein (LDL) receptor-1 (LOX-1) expression in atherosclerotic lesions is associated with tissue factor expression and apoptosis in hypercholesterolemic rabbits. *Biol Pharm Bull.* 2008;31:1475–1482.
6. Shiomi M, Ito T, Yamada S, Kawashima S, Fan J. Development of an animal model for spontaneous myocardial infarction (WHHLMI rabbit). *Arterioscler Thromb Vasc Biol.* 2003;23:1239–1244.
7. Abrams MJ, Juweid M, tenKate CI, et al. Technetium-99m-human polyclonal IgG radiolabeled via the hydrazino nicotinamide derivative for imaging focal sites of infection in rats. *J Nucl Med.* 1990;31:2022–2028.
8. Ono M, Arano Y, Mukai T, et al. Plasma protein binding of ^{99m}Tc-labeled hydrazino nicotinamide derivatized polypeptides and peptides. *Nucl Med Biol.* 2001;28:155–164.
9. Larsen SK, Solomon HF, Caldwell G, Abrams MJ. [^{99m}Tc]tricine: a useful precursor complex for the radiolabeling of hydrazinonicotinate protein conjugates. *Bioconjug Chem.* 1995;6:635–638.
10. Ishii K, Kita T, Kume N, Nagano Y, Kawai C. Uptake of acetylated LDL by peritoneal macrophages obtained from normal and Watanabe heritable hyperlipidemic rabbits, an animal model for familial hypercholesterolemia. *Biochim Biophys Acta.* 1988;962:387–389.
11. Ogawa M, Ishino S, Mukai T, et al. ^{18}F-FDG accumulation in atherosclerotic plaques: immunohistochemical and PET imaging study. *J Nucl Med.* 2004;45:1245–1250.
12. Stary HC, Chandler AB, Glagov S, et al. A definition of initial, fatty streak, and intermediate lesions of atherosclerosis: a report from the Committee on Vascular Lesions of the Council on Arteriosclerosis, American Heart Association. *Circulation.* 1994;89:2462–2478.
13. Stary HC, Chandler AB, Dinsmore RE, et al. A definition of advanced types of atherosclerotic lesions and a histological classification of atherosclerosis: a report from the Committee on Vascular Lesions of the Council on Arteriosclerosis, American Heart Association. *Circulation.* 1995;92:1355–1374.
14. Kobayashi S, Inoue N, Ohashi Y, et al. Interaction of oxidative stress and inflammatory response in coronary plaque instability: important role of C-reactive protein. *Arterioscler Thromb Vasc Biol.* 2003;23:1398–1404.
15. Ishino S, Kuge Y, Takai N, et al. ^{99m}Tc-Annexin A5 for noninvasive characterization of atherosclerotic lesions: imaging and histological studies in myocardial infarction-prone Watanabe heritable hyperlipidemic rabbits. *Eur J Nucl Med Mol Imaging.* 2007;34:889–899.
16. Shiomi M, Ito T, Hirouchi Y, Enomoto M. Stability of atheromatous plaque affected by lesional composition: study of WHHL rabbits treated with statins. *Ann N Y Acad Sci.* 2001;947:419–423.
17. Ishino S, Mukai T, Kuge Y, et al. Targeting of lectinlike oxidized low-density lipoprotein receptor 1 (LOX-1) with ^{99m}Tc-labeled anti-LOX-1 antibody: potential agent for imaging of vulnerable plaque. *J Nucl Med.* 2008;49:1677–1685.
18. Shiomi M, Ito T, Hirouchi Y, Enomoto M. Fibromuscular cap composition is important for the stability of established atherosclerotic plaques in mature WHHL rabbits treated with statins. *Atherosclerosis.* 2001;157:75–84.
19. Huhalov A, Chester KA. Engineered single chain antibody fragments for radioimmunotherapy. *Q J Nucl Med Mol Imaging.* 2004;48:279–288.
20. Sharkey RM, Karacay H, Cardillo TM, et al. Improving the delivery of radionuclides for imaging and therapy of cancer using pretargeting methods. *Clin Cancer Res.* 2005;11:7109s–7121s.
21. Sano K, Temma T, Kuge Y, et al. Radioimmunodetection of membrane type-1 matrix metalloproteinase relevant to tumor malignancy with a pre-targeting method. *Biol Pharm Bull.* 2010;33:1589–1595.
22. Temma T, Iida H, Hayashi T, et al. Quantification of regional myocardial oxygen metabolism in normal pigs using positron emission tomography with injectable ^{15}O-O_2. *Eur J Nucl Med Mol Imaging.* 2010:37:377–385.
23. Yamamoto Y, de Silva R, Rhodes CG, et al. Noninvasive quantification of regional myocardial metabolic rate of oxygen by $^{15}O_2$ inhalation and positron emission tomography: experimental validation. *Circulation.* 1996;94:808–816.
24. Iida H, Rhodes CG, Araujo LI, et al. Noninvasive quantification of regional myocardial metabolic rate for oxygen by use of $^{15}O_2$ inhalation and positron emission tomography: theory, error analysis, and application in humans. *Circulation.* 1996;94:792–807.
25. Watabe H, Ikoma Y, Kimura Y, Naganawa M, Shidahara M. PET kinetic analysis: compartmental model. *Ann Nucl Med.* 2006;20:583–588.
26. Ikoma Y, Watabe H, Shidahara M, Naganawa M, Kimura Y. PET kinetic analysis: error consideration of quantitative analysis in dynamic studies. *Ann Nucl Med.* 2008;22:1–11.
27. Rogers BE, Anderson CJ, Connett JM, et al. Comparison of four bifunctional chelates for radiolabeling monoclonal antibodies with copper radioisotopes: biodistribution and metabolism. *Bioconjug Chem.* 1996;7:511–522.
28. Sugimoto K, Nishimoto N, Kishimoto T, Yoshizaki K, Nishimura T. Imaging of lesions in a murine rheumatoid arthritis model with a humanized anti-interleukin-6 receptor antibody. *Ann Nucl Med.* 2005;19:261–266.
29. D'Alessandria C, Malviya G, Viscido A, et al. Use of a ^{99m}Tc labeled anti-TNFα monoclonal antibody in Crohn's disease: in vitro and in vivo studies. *Q J Nucl Med Mol Imaging.* 2007;51:334–342.
30. Akizawa H, Arano Y. Altering pharmacokinetics of radiolabeled antibodies by the interposition of metabolizable linkages: metabolizable linkers and pharmacokinetics of monoclonal antibodies. *Q J Nucl Med.* 2002;46:206–223.
31. Campean V, Neureiter D, Varga I, et al. Atherosclerosis and vascular calcification in chronic renal failure. *Kidney Blood Press Res.* 2005;28:280–289.
32. Drake TA, Morrissey JH, Edgington TS. Selective cellular expression of tissue factor in human tissues: implications for disorders of hemostasis and thrombosis. *Am J Pathol.* 1989;134:1087–1097.
33. Prezelj A, Anderluh PS, Peternel L, Urleb U. Recent advances in serine protease inhibitors as anticoagulant agents. *Curr Pharm Des.* 2007;13:287–312.
34. Davies JR, Rudd JH, Weissberg PL, Narula J. Radionuclide imaging for the detection of inflammation in vulnerable plaques. *J Am Coll Cardiol.* 2006;47(8, suppl):C57–C68.
35. Jaffer FA, Libby P, Weissleder R. Molecular and cellular imaging of atherosclerosis: emerging applications. *J Am Coll Cardiol.* 2006;47:1328–1338.
36. Rudd JH, Hyafil F, Fayad ZA. Inflammation imaging in atherosclerosis. *Arterioscler Thromb Vasc Biol.* 2009:29:1009–1016.
37. Zhao Y, Kuge Y, Zhao S, et al. Comparison of ^{99m}Tc-annexin A5 with ^{18}F-FDG for the detection of atherosclerosis in ApoE−/− mice. *Eur J Nucl Med Mol Imaging.* 2007;34:1747–1755.

Erratum

In the article "^{18}F-FDG PET After 2 Cycles of ABVD Predicts Event-Free Survival in Early and Advanced Hodgkin Lymphoma," by Cerci et al. (*J Nucl Med.* 2010;51:1337–1343), Figure 4 contained a mistake. The graph of event-free survival in patients with a low International Prognostic Score should indicate that 10 of 18 patients (not 3 of 30) were PET2-positive. The authors regret the error.

Radioimmunodetection of Membrane Type-1 Matrix Metalloproteinase Relevant to Tumor Malignancy with a Pre-targeting Method

Kohei SANO,[a] Takashi TEMMA,[a] Yuji KUGE,*[a,b,c] Takashi KUDO,[a] Junko KAMIHASHI,[a] Songji ZHAO,[b] and Hideo SAJI[a]

[a] *Department of Patho-Functional Bioanalysis, Graduate School of Pharmaceutical Sciences, Kyoto University; 46–29 Yoshida Shimoadachi-cho, Sakyo-ku, Kyoto 606–8501, Japan:* [b] *Department of Tracer Kinetics & Bioanalysis, Graduate School of Medicine, Hokkaido University; and* [c] *Central Institute of Isotope Science, Hokkaido University; Kita 15 Nishi 7, Kita-ku, Sapporo 060–8638, Japan.* Received April 5, 2010; accepted June 28, 2010; published online June 30, 2010

Since membrane type-1 matrix metalloproteinase (MT1-MMP) is exclusively expressed in tumors and is closely associated with metastasis and invasion, MT1-MMP is a potential target of radiotracers for the evaluation of tumor malignancy. In this study, we planned to visualize MT1-MMP *in vivo* by a two-step pre-targeting strategy using a streptavidin (SAv)-biotin system combined with anti-MT1-MMP monoclonal immunoglobulin (IgG) (anti-MT1-MMP monoclonal antibody (mAb)). Streptavidinylated anti-MT1-MMP mAb was synthesized by reacting biotinylated anti-MT1-MMP mAb with SAv. In the pre-targeting study, FM3A mouse breast carcinoma-implanted mice were injected with anti-MT1-MMP mAb-SAv, followed 72 h later with radioiodinated biotin, (3-[$^{123/125}$I]iodobenzoyl)norbiotinamide ($^{123/125}$I-IBB). Biodistribution and imaging (single photon emission computed tomography (SPECT)/CT) data were collected at several time points in the 24 h period following introduction of the tracer. The comparison groups were injected with ^{125}I-IBB alone or with ^{125}I-IBB pre-targeted with negative control IgG-SAv. In the pre-targeting study for MT1-MMP, within 1 h of tracer injection, rapid tumor uptake and abrupt clearance from the blood of radioactivity (2.22, 0.87% injected dose/g at 1 h) were observed. The tumor to blood (T/B) radioactivity ratios were significantly higher than those from mice dosed with the pre-targeting negative control ($p<0.0001$). ^{125}I-IBB alone did not accumulate in tumors. SPECT/CT image analysis of FM3A bearing mice showed high-contrast tumor images after 3 h with minimal blood-pool activity. The present study that uses a pre-targeting method showed high T/B radioactivity ratios and clear tumor images of MT1-MMP. This imaging method may be useful for the clinical diagnosis of malignant tumors.

Key words membrane type-1 matrix metalloproteinase; pre-targeting; non-invasive imaging; streptavidin; biotin; malignant tumor

Tumor malignancy is closely associated with the poor prognosis in cancer patients. Thus, accurate and sensitive diagnosis for detecting the tumor malignancy is required to provide the optimal therapeutic regimen to the patients. Nuclear medical techniques such as single photon emission computed tomography (SPECT) and positron emission tomography (PET) are non-invasive and have the potential to provide sensitive diagnoses by detecting gamma rays emitted from a radiolabeled probe injected into the body. Thus, a radiolabeled probe targeted to a biological molecule relevant to tumor malignancy can be a useful tool for detecting the malignant tumors.

Matrix metalloproteinases (MMPs), classified as secreted MMPs and membrane-associated MMPs (membrane type MMPs, MT-MMPs) based on their structures,[1)] play important roles in tumor growth, invasion, and metastasis by degrading most of the components in the extracellular matrix.[2)] Membrane type-1 MMP (MT1-MMP) in particular is considered to be closely associated with tumor malignancy. Indeed, recent studies have shown that MT1-MMP activates MMP-2, an effector protease that operates downstream of MT1-MMP.[1,3—6)] In addition, expression of MT1-MMP is localized to tumor tissues[1)] and increases in the early stages of tumorigenesis.[7)] Thus, MT1-MMP is a potential target for imaging malignant tumors at an early phase in their development.

Recently, we proposed ^{99m}Tc-labeled anti-MT1-MMP monoclonal immunoglobulin (IgG) (^{99m}Tc-anti-MT1-MMP monoclonal antibody (mAb)) as a novel MT1-MMP probe and demonstrated its effectiveness for evaluating the malignancy of breast tumors in rodent models.[8)] However, the blood clearance of ^{99m}Tc-anti-MT1-MMP mAb was not fast enough to obtain a high tumor to blood (T/B) ratio, an indicator of availability of radiotracer for *in vivo* imaging, during the first hours following administration. The T/B ratio remained low at 48 h post-injection, which prevents the achievement of MT1-MMP imaging *in vivo*. For future clinical applications, this probe should be modified to improve the MT1-MMP imaging sensitivity and to provide earlier post-injection imaging.

For this purpose, we planed to use a pre-targeting method combined with the anti-MT1-MMP mAb. The pre-targeting method, extensively studied in the field of radioimmunotherapy, can provide selective accumulation of radioactivity to the targeted organ and a high signal-to-noise (S/N) ratio during the first hours following administration.[9,10)] Recently, publications have reported that the pre-targeting method, utilizing an interaction between bispecific antibodies and haptens, is applicable to *in vivo* molecular imaging.[11,12)] Here, we exploited a streptavidin–biotin system possessing high affinity ($K_d=10^{-15}$ M)[13)] for *in vivo* binding of pre- and post-administered compounds and applied this pre-targeting method to MT1-MMP imaging.

This study sought to determine the effectiveness of a pre-targeting protocol (streptavidinylated anti-MT1-MMP mAb and radiolabeled biotin) for MT1-MMP imaging shortly after administration of a radiolabeled probe, through biodistribution studies and *in vivo* SPECT imaging. Among tumor types, breast cancer remains a predominant cause of death in women despite advances in treatment, especially in cases where distant metastases occur.[14)] This motivated us to select

* To whom correspondence should be addressed. e-mail: kuge@ric.hokudai.ac.jp

breast cancer as the target disease for investigation of the MT1-MMP probe.

MATERIALS AND METHODS

Cell Lines and Animal Models Female C3H/He mice (5 weeks old), supplied by Japan SLC, Inc. (Hamamatsu, Japan), were housed under a 12 h light/12 h dark cycle and were given free access to a biotin-deficient diet and water. The animal experiments in this study were conducted in accordance with institutional guidelines and approved by the Kyoto University Animal Care Committee, Japan.

The mouse breast carcinoma FM3A cell line, supplied by Health Science Research Resources Bank (Osaka, Japan), was used for the preparation of tumor-bearing animal models. The cells were grown in Dulbecco's modified Eagle's medium (Nissui Pharmaceutical Co., Japan) containing 10% fetal bovine serum and were maintained in a humidified atmosphere of 5% CO_2 and 95% air at 37 °C with a 10.6 h doubling time.

FM3A cells were suspended in 0.01 M phosphate buffered saline (PBS) (pH 7.4) followed by subcutaneous inoculation into the right thigh of mice (5×10^6 cells/100 μl PBS/mouse). Individual tumor volumes (V) were estimated as $V=ab^2/2$, where a is the larger diameter and b is the smaller diameter.[15] Biodistribution studies were performed 7—8 d after implantation. The tumor volume was 155 ± 78 mm^3. The expression of MT1-MMP in FM3A cells and tumor tissues was confirmed by western blotting and immunohistochemistry.[8]

Synthesis of Biotinylated Anti-MT1-MMP mAb Anti-MT1-MMP mAb (113-5B7, Daiichi Fine Chemical Co., Japan), a purified mouse monoclonal IgG_3 to an oligopeptide, residues 319 to 333 of human MT1-MMP numbered from the signal peptide, was used for experiments after purification with a HiTrap rProtein A column (GE Healthcare, U.K.). Since the amino acid sequence of the MT1-MMP protein is highly conserved among species including mouse, rat, rabbit, and human,[16] this antibody can cross-react with mouse as well as human MT1-MMP.[17]

EZ-Link® sulfosuccinimidyl-6-(biotinamido) hexanoate (sulfo-NHS-LC-biotin) (Pierce, Inc., U.S.A.) (105 μl, 1.0 mg/ml in 0.1 M PBS (pH 7.4)) was added to a solution of anti-MT1-MMP mAb (2.4 ml, 1.0 mg/ml in 0.1 M PBS (pH 7.4)) in a molar ratio of 12 : 1. The mixture was gently stirred for 30 min at room temperature and then was purified with a diafiltration membrane (Amicon Ultra 4 (MWCO 30000), Millipore Co., U.S.A.). The mean substitution ratio for biotin molecules coupled to the antibody was determined by the EZ™ Biotin Quantitation Kit (Pierce, Inc.) using 4-hydroxyazobenzene-2′-carboxylic acid (HABA). The immunoreactivity of biotinylated anti-MT1-MMP mAb was measured using flow cytometry as previously described.[18] In brief, the antibody (50 μg/ml, 100 μl) (anti-MT1-MMP mAb, biotinylated anti-MT1-MMP mAb or negative control IgG_3 (sc-3880, Santa Cruz Biotechnology, Inc., U.S.A.) was added to mouse macrophage cells (RAW264.7, 2×10^6 cells) and was incubated for 30 min on ice, followed by incubation with FITC-Alexa-Fluor® 488 goat anti-mouse IgG antibody (A-11001, Molecular Probes, Inc., U.S.A.) (10 μg/ml, 100 μl) for 30 min on ice. The fluorescence level was measured using a flow cytometer (Becton Dickinson Inc., U.S.A.), and the data were analyzed using BD CellQuest Pro (BD Biosciences Inc., U.S.A.). An index of immunoreactivity for the anti-MT1-MMP mAb and biotinylated anti-MT1-MMP mAb was calculated by the following equation: median fluorescence intensity of anti-MT1-MMP mAb or biotinylated anti-MT1-MMP mAb divided by median fluorescence intensity of the negative control IgG.

Preparation and Purification of Anti-MT1-MMP mAb-SAv Conjugate A solution of biotinylated anti-MT1-MMP mAb (1.93 ml, 1 mg/ml in PBS) was added to a solution of streptavidin (SAv) (2.32 mg) (Pierce, Inc.) in a 1 : 3 molar ratio. The mixture was incubated for 1 h at 37 °C followed by purification twice by affinity chromatography using a HiTrap rProtein A column. The eluate containing anti-MT1-MMP mAb-SAv was concentrated with a diafiltration membrane (MWCO 30000), and the protein concentration was determined by the bicinchoninate (BCA) method. The purification was monitored by size exclusion chromatography using a 300×4.6 mm i.d. TSK-Gel Super SW 3000 column (Tosoh Co., Japan) eluted with phosphate buffer (0.1 M, pH 6.8) at a flow rate of 0.3 ml/min. Comparison to molecular mass standards (Oriental Yeast Co., Japan) of the absorbance at 280 nm indicated that a peak at 9.1 min was consistent with the presence of the 210 kDa anti-MT1-MMP mAb-SAv. Anti-MT1-MMP mAb-SAv was obtained in a yield of 36%. Negative control IgG-SAv was synthesized by the same procedure as described above in 62% yield.

Radioiodination of Biotin (3-[$^{123/125}$I]Iodobenzoyl)norbiotinamide ($^{123/125}$I-IBB) was synthesized according to the synthetic procedure outlined by Foulon *et al.*[19] with some modifications. Briefly, to a vial containing *N*-succinimidyl 3-(tributylstannyl)benzoate (72.2 μl, 2 mg/ml in methanol (1% acetic acid)) were added *N*-chlorosuccinimide (19.8 μl, 0.5 mg/ml in methanol) and concentrated $NH_4{}^{123}I$ (1110 MBq) or $Na^{125}I$ (37 MBq). The vial was vortexed, and the reaction was allowed to proceed for 30 min at room temperature. The reaction was quenched by the addition of $NaHSO_3$ (3.2 μl, 0.72 mg/ml in water), the solvent was evaporated under a stream of nitrogen, and the residue was used directly for the next reaction. A solution of norbiotinamine·HCl (Molecular Probes, Inc.) (100 μl, 3 mg/ml in *N*,*N*-dimethylformamide : water=4 : 1, pH 8.5—9.0) was added to a vial containing the $^{123/125}$I-*N*-succinimidyl 3-iodobenzoate ($^{123/125}$I-SIB) synthesized above, and the reaction was incubated for 2 h at room temperature. The product was purified by reverse-phase high-performance liquid chromatography (HPLC) using a Cosmosil $5C_{18}$-AR-300 Packed Column, 150×4.6 mm i.d. (Nacalai Tesque, Inc., Kyoto, Japan), eluting with acetonitrile : water=25 : 75 at a flow rate of 1.0 ml/min (retention time was 18 min for $^{123/125}$I-IBB). The radiochemical purity was determined by thin-layer chromatography on a silica gel plate with chloroform : methanol=6 : 1 (Rf=0.53) as eluent and by analytical HPLC under the same conditions as above. $^{123/125}$I-IBB was obtained in a radiochemical yield of 21% and 39% and a radiochemical purity of more than 94% and 95%, respectively.

Synthesis of ^{125}I Labeled Anti-MT1-MMP mAb-SAv Conjugation of ^{125}I-SIB with streptavidin was performed according to the procedure of Zalutsky and Narula[20] with slight modifications as follows: a solution of streptavidin (300 μl, 20 mg/ml in 0.15 M borate buffer (pH 8.5)) was

added to the dried residue of crude ^{125}I-SIB (32.6 MBq). After gentle agitation for 30 min at room temperature, the radioiodinated streptavidin was applied to a diafiltration membrane to remove unbound ^{125}I-SIB as well as to change buffer to PBS (0.1 M, pH 7.4). To a vial containing purified ^{125}I-streptavidin (18.5 MBq, 2.6 ml, 1.1 mg/ml in PBS), a solution of MT1-MMP mAb-Bt (1.0 ml, 3.6 mg/ml in PBS) was added, and the reaction was incubated for 1 h at room temperature followed by purification twice by affinity chromatography using a HiTrap rProtein A column. The eluate containing ^{125}I-SAv-anti-MT1-MMP mAb was concentrated with a diafiltration membrane. The protein concentration was determined by the BCA method. ^{125}I-SAv-anti-MT1-MMP mAb was obtained in a radiochemical yield of 11% and a radiochemical purity of more than 94%.

***In Vivo* Biodistribution Study** Mice were divided into 4 groups (n=3—9) for 4 or 5 time points with approximately equal distribution of tumor sizes on the day before the study. Animals were fasted for 6 h before administration of the radiopharmaceutical. Outline of the each biodistribution study is shown in Fig. 1.

One, 6, 24, 48, and 72 h after the injection of ^{125}I-SAv-anti-MT1-MMP mAb (90 kBq, 50 μg/100 μl in saline), the blood, heart, lung, liver, kidney, intestine, pancreas, spleen, muscle, brain, and tumor were excised, weighed, and counted for radioactivity with a NaI well-type scintillation counter (1470WIZARD, PerkinElmer Japan Co.) using the injected dose as a standard. Data were calculated as % injected dose (ID)/g of tissue and %ID/organ.

In the pre-targeting, ^{125}I-IBB (110 kBq, 100 μl in saline) was injected intravenously into mice 72 h after pre-treatment with anti-MT1-MMP mAb-SAv (50 μg/100 μl in saline). One, 3, 6, and 24 h after the injection of ^{125}I-IBB, the biodistribution was evaluated as described above. The biodistribution of ^{125}I-IBB alone and ^{125}I-IBB pre-targeted with negative control IgG-SAv (50 μg/100 μl in saline) were also evaluated 1, 3, 6, and 24 h post-injection in the same manner.

***In Vivo* Imaging Studies** The SPECT studies were performed using a SPECT-2000H-40 gamma camera (Hitachi Medical Co.). Mice (n=2) bearing an FM3A tumor in the right thigh received anti-MT1-MMP mAb-SAv (50 μg/100 μl in saline) *via* the tail vein. Three days later, ^{123}I-IBB (62.9 MBq/100 μL in saline) was injected followed by data acquisition as static SPECT scans (360° rotation, 30 s/step for 64 steps) using low-energy high-resolution, parallel-hole collimators (30% window, 159 keV energy peak, 128×128 matrix mode, pixel size of 2.0 mm) at 3, 6, and 24 h post injection under halothan (1.5%) anesthesia. Images were reconstructed with a standard filtered back projection algorithm.

After the SPECT scans, X-ray images of the mice were obtained for an anatomical comparison using an R-mCT system (Rigaku Co.) equipped with a fixed microfocus X-ray tube and X-ray sensor. This instrument exposes a cone-shaped X-ray beam on the 2D detector through the animal set on a stage. The revolving arm rotates 360° around the mouse for 17 s to acquire a full 3D computerized tomography (CT) data set.

Statistical Analysis To compare the time courses of radioactivity in the tumor, tumor to blood (T/B) and tumor to muscle (T/M) ratios among anti-MT1-MMP mAb-SAv pre-targeted ^{125}I-IBB, negative control IgG-SAv pre-targeted ^{125}I-IBB and ^{125}I-IBB alone, two-way factorial ANOVA followed by a Tukey–Kramer test was performed. Differences at the 95% confidence level (p<0.05) were considered significant.

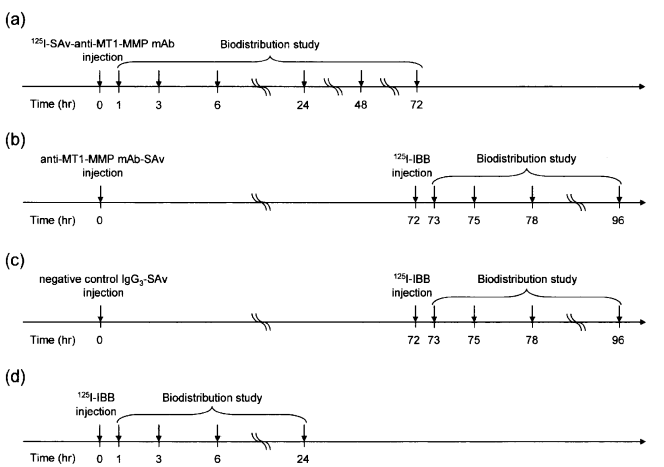

Fig. 1. Outline of the Biodistribution Studies

(a) ^{125}I-SAv-anti-MT1-MMP mAb, (b) ^{125}I-IBB pre-targeted with anti-MT1-MMP mAb-SAv, (c) ^{125}I-IBB pre-targeted with negative control IgG_2-SAv, and (d) ^{125}I-IBB alone. In each time point, biodistribution studies were conducted.

Table 1. Biodistribution of Radioactivity after the Injection of ^{125}I-SAv-anti-MT1-MMP mAb in C3H/He Mice Bearing FM3A Mouse Breast Tumors[a)]

	Time after injection (h)				
	1 (n=3)	6 (n=3)	24 (n=4)	48 (n=3)	72 (n=4)
Blood	40.65±0.44	25.29±2.47	11.93±0.88	7.27±0.35	5.62±0.51
Heart	5.71±1.31	4.58±0.42	2.88±0.38	2.10±0.06	2.04±0.36
Lung	18.35±4.28	11.88±1.71	6.36±1.16	6.63±4.06	3.55±0.68
Liver	9.36±0.43	9.32±1.23	5.89±0.34	5.70±0.54	5.63±0.67
Kidney	7.39±0.77	7.77±1.07	8.71±0.68	9.59±0.36	10.56±0.69
Intestine	1.85±0.05	2.90±0.34	1.59±0.19	1.04±0.10	0.92±0.06
Pancreas	1.12±0.17	1.44±0.30	1.22±0.14	1.02±0.08	1.23±0.12
Spleen	30.05±9.46	23.20±1.73	16.89±0.67	13.47±2.11	12.70±1.62
Muscle	0.58±0.13	0.59±0.10	0.84±0.16	0.63±0.10	0.74±0.13
Brain	0.71±0.04	0.53±0.12	0.22±0.03	0.18±0.02	0.14±0.01
Tumor	2.81±0.45	5.47±0.81	7.69±0.42	6.34±0.65	5.78±0.94
Tumor/blood	0.07±0.01	0.22±0.05	0.65±0.05	0.88±0.11	1.03±0.13
Tumor/muscle	5.16±2.11	9.48±2.44	9.44±1.78	10.31±2.22	7.87±0.26
Stomach[b)]	0.16±0.03	0.35±0.05	0.29±0.02	0.21±0.05	0.16±0.09
Urine[b,c)]			7.99±3.92	34.09±8.49	38.23±9.28
Feces[b,c)]			1.58±1.60	11.79±3.25	12.41±3.23

a) Tissue radioactivity is expressed as % injected dose per gram. Each value represents the mean±S.D. for three (1, 6, 48 h) and four (24, 72 h) animals. *b*) Expressed as % injected dose. *c*) Calculated using summated radioactivity of four animals (72 h group).

RESULTS

Immunoreactivity of Biotinylated Anti-MT1-MMP mAb The number of conjugated biotins per antibody was 2.2±0.5 when the reaction ratio of anti-MT1-MMP mAb and biotin was 1 : 12. The indices of immunoreactivity evaluated by the flow cytometry analyses were 5.8±0.9 and 6.1±1.0 for the biotinylated anti-MT1-MMP mAb and the intact anti-MT1-MMP mAb, respectively. The immunoreactivity of the anti-MT1-MMP mAb was not affected by the introduction of biotins into the anti-MT1-MMP mAb (greater than 90% retained).

Biodistribution Studies To determine the timing for post-administration, a biodistribution study of ^{125}I-SAv-anti-MT1-MMP mAb was performed first (Table 1). Radioactivity in the tumor reached a peak at 24 h (7.69% ID/g) and gradually decreased (6.34% ID/g at 48 h and 5.78% ID/g at 72 h). The kidney and spleen showed rather high radioactivity over time (10.56, 12.70% ID/g at 72 h, respectively). The T/B ratios increased in a time-dependent manner and reached greater than 1.0 at 72 h after injection. Therefore, taking into consideration radioactivity in the tumor and T/B ratios, an interval of 72 h was selected for the subsequent pre-targeting study.

Results of *in vivo* biodistribution studies of ^{125}I-IBB with pre-targeting using the anti-MT1-MMP mAb-SAv or negative control IgG-SAv are summarized in Tables 2 and 3. In the pre-targeting study targeting MT1-MMP (Table 2), ^{125}I-IBB was highly accumulated in the tumor at 3 h (2.36% ID/g) and a high level was maintained for 24 h after the injection (1.06% ID/g at 24 h) while blood clearance was rapid (0.47, 0.07% ID/g at 3, 24 h, respectively), resulting in high T/B ratios of ^{125}I-IBB early after the injection (2.55 at 1 h, 5.36 at 3 h, 7.78 at 6 h, 14.13 at 24 h). T/M ratios increased in a similar manner (3.09 at 1 h, 6.14 at 3 h, 6.99 at 6 h, 12.09 at 24 h). Other organs with the exception of the kidneys, intestine and spleen showed low radioactivity 24 h after the injection.

Radioactivity in the tumor was significantly lower (0.66% ID/g at 24 h) in the control pre-targeting study (Table 3) than in the actual pre-targeting study (p<0.0005), and the blood clearance was slightly slower (0.08% ID/g at 24 h). T/B ratios were significantly higher with the true pre-targeting method as compared to the control pre-targeting method (p<0.0001) (Fig. 2). T/M ratios were also higher with the true pre-targeting method, although these values were not significantly different between the groups. The biodistribution to other tissues, including the kidneys, intestine, spleen and liver, was similar between the groups.

In the biodistribution study of ^{125}I-IBB alone (Table 4), negligible accumulation in the tumor (0.15, <0.01% ID/g at 3, 24 h, respectively) and an extremely rapid blood clearance (0.33, 0.03% ID/g at 3, 24 h, respectively) were observed. T/B and T/M ratios were small over time (0.44, 0.58 at 1 h,

Table 2. Biodistribution of Radioactivity after the Injection of ^{125}I-IBB in C3H/He Mice Bearing FM3A Mouse Breast Tumors, Pre-targeted with Anti-MT1-MMP mAb-SAv[a)]

	Time after injection (h)			
	1 (n=9)	3 (n=8)	6 (n=9)	24 (n=9)
Blood	0.87±0.12	0.47±0.12	0.26±0.08	0.07±0.02
Heart	1.26±0.12	0.75±0.08	0.49±0.06	0.16±0.04
Lung	1.61±0.19	0.98±0.24	0.55±0.10	0.14±0.05
Liver	8.11±1.20	4.35±0.51	3.31±0.49	0.92±0.33
Kidney	73.74±6.56	62.82±11.40	45.98±6.85	20.99±3.47
Intestine	19.33±2.11	23.54±4.99	24.78±5.19	2.21±1.37
Pancreas	1.78±0.54	0.89±0.17	0.62±0.10	0.15±0.03
Spleen	9.74±2.16	8.25±1.23	6.37±2.13	2.09±1.56
Muscle	0.76±0.16	0.39±0.07	0.28±0.06	0.09±0.02
Brain	0.04±0.03	0.02±0.00	0.01±0.00	0.00±0.00
Tumor	2.22±0.58	2.36±0.78	1.89±0.27	1.06±0.39
Tumor/blood	2.55±0.52	5.36±2.49	7.78±1.79	14.13±3.51
Tumor/muscle	3.09±1.27	6.14±2.02	6.99±1.42	12.09±5.95
Stomach[b)]	0.79±0.39	0.50±0.24	0.29±0.11	0.14±0.10
Urine[b)]				23.02±10.16
Feces[b)]				18.15±4.01

a) Tissue radioactivity is expressed as % injected dose per gram. Each value represents the mean±S.D. for three (6, 24 h) and four (1, 3 h) animals. *b*) Expressed as % injected dose.

Table 3. Biodistribution of Radioactivity after the Injection of ^{125}I-IBB in C3H/He Mice Bearing FM3A Mouse Breast Tumors, Pre-targeted with Negative Control IgG-SAv[a)]

	Time after injection (h)			
	1 (n=6)	3 (n=4)	6 (n=5)	24 (n=6)
Blood	1.04±0.05	0.58±0.01	0.34±0.06	0.08±0.01
Heart	1.16±0.11	0.74±0.06	0.56±0.08	0.15±0.03
Lung	2.13±0.34	1.27±0.17	0.84±0.16	0.17±0.03
Liver	7.61±1.25	4.79±0.59	3.69±0.62	1.26±0.37
Kidney	60.71±10.23	52.12±5.09	41.26±5.34	12.87±2.15
Intestine	13.37±1.85	18.35±1.73	22.72±2.50	2.12±1.21
Pancreas	1.32±0.11	0.78±0.08	0.57±0.06	0.13±0.05
Spleen	10.89±1.65	9.82±1.37	8.07±1.91	4.32±1.28
Muscle	0.64±0.04	0.34±0.08	0.29±0.06	0.10±0.02
Brain	0.03±0.00	0.02±0.00	0.01±0.00	0.00±0.00
Tumor	1.75±0.23	1.63±0.32	1.43±0.45	0.66±0.08
Tumor/blood	1.68±0.20	2.84±0.59	4.19±0.59	8.80±0.70
Tumor/muscle	2.75±0.36	4.91±1.24	4.95±1.29	7.17±1.60
Stomach[b)]	0.30±0.08	2.42±1.96	1.20±1.20	0.45±0.65
Urine[b)]				11.95±9.27
Feces[b)]				18.59±7.93

a) Tissue radioactivity is expressed as % injected dose per gram. Each value represents the mean±S.D. for four (3 h), five (6 h) and six (1, 24 h) animals. *b*) Expressed as % injected dose.

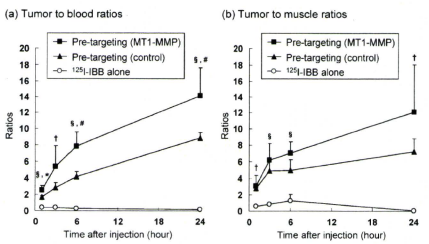

Fig. 2. (a) Tumor to Blood Ratios and (b) Tumor to Muscle Ratios of Radioactivity after the Administration of ^{125}I-IBB (Open Circle), ^{125}I-IBB Following Anti-MT1-MMP mAb-SAv (Closed Square) and ^{125}I-IBB Following Negative Control IgG-SAv (Closed Triangle)

Data are presented as the mean±S.D. Comparisons among groups were performed by two-way factorial ANOVA followed by a Tukey–Kramer test. $*p<0.05$, $*p<0.01$ *vs.* ^{125}I-IBB following negative control IgG-SAv and $\dagger p<0.05$, $\S p<0.01$ *vs.* ^{125}I-IBB.

Table 4. Biodistribution of Radioactivity after the Injection of ^{125}I-IBB in C3H/He Mice Bearing FM3A Mouse Breast Tumors[a)]

	Time after injection (h)			
	1 (n=4)	3 (n=4)	6 (n=3)	24 (n=3)
Blood	1.17±0.48	0.33±0.01	0.15±0.00	0.03±0.00
Heart	1.37±0.25	0.29±0.06	0.07±0.06	0.03±0.02
Lung	1.24±0.10	0.32±0.04	0.11±0.02	0.02±0.00
Liver	6.07±1.81	1.34±0.26	0.20±0.03	0.03±0.01
Kidney	5.61±0.84	1.02±0.20	0.42±0.21	0.08±0.01
Intestine	35.09±7.01	22.79±10.63	10.20±6.90	1.34±0.49
Pancreas	1.26±0.44	0.34±0.12	0.05±0.01	0.00±0.02
Spleen	0.56±0.07	0.13±0.05	0.04±0.04	0.02±0.04
Muscle	0.85±0.21	0.18±0.08	0.04±0.02	0.04±0.03
Brain	0.03±0.01	0.01±0.01	0.00±0.00	0.00±0.00
Tumor	0.50±0.13	0.14±0.04	0.04±0.00	0.00±0.00
Tumor/blood	0.44±0.09	0.42±0.10	0.30±0.03	0.16±0.14
Tumor/muscle	0.58±0.06	0.82±0.18	1.29±0.74	0.05±0.04
Stomach[b)]	4.03±1.27	1.17±0.82	0.24±0.18	0.37±0.35

a) Tissue radioactivity is expressed as % injected dose per gram. Each value represents the mean±S.D. for three (6, 24 h) and four (1, 3 h) animals. *b*) Expressed as % injected dose.

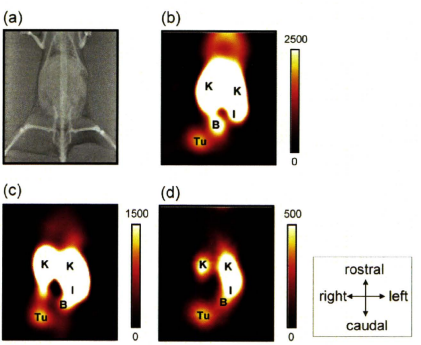

Fig. 3. X-Ray CT (a) and SPECT Images (b—d) in the Coronal Plane at 3, 6, and 24 h after the Injection of ^{123}I-IBB Pre-targeted with Anti-MT1-MMP mAb-SAv in a C3H/He Mouse Bearing an FM3A Mouse Breast Tumor

Photographs (b—d) are slices at the level of tumor and kidneys. Tu, K, I, and B indicate the tumor, kidney, intestine and bladder, respectively. SPECT images clearly visualize the tumor in the right thigh.

0.42, 0.82 at 3 h, 0.30, 1.29 at 6 h, 0.16, 0.05 at 24 h, respectively). ^{125}I-IBB mainly accumulated in the intestine, followed by the kidneys and liver shortly after injection.

Imaging Studies Figure 3 shows X-ray CT (a) and SPECT images at 3 (b), 6 (c) and 24 (d) h after injection of ^{123}I-IBB in FM3A-implanted mice pre-targeted with anti-MT1-MMP mAb-SAv. The location of each tissue in the SPECT images is referenced to the X-ray CT image. The tumor was clearly visualized at 3 h after administration of ^{123}I-IBB and the accumulation of radioactivity in the tumor was maintained for 24 h. Though the kidneys, bladder and intestine were also visualized, the radioactivity in these tissues decreased relatively quickly over time compared with that in the tumor. Chest organs such as the lungs and heart, and the liver were not visualized. The distribution of signals in each tissue was very consistent with the distribution of radioactivity observed in the *in vivo* biodistribution study (Table 2).

DISCUSSION

In this study, we developed a novel MT1-MMP imaging method based on anti-MT1-MMP mAb combined with a pre-targeting strategy using a biotin–streptavidin system. The effectiveness of this pre-targeting method (streptavidinylated anti-MT1-MMP mAb and $^{123/125}$I-IBB) was validated since significantly higher T/B ratios were achieved during the first hours after administration than had been observed in our previous study using a directly labeled antibody,[8)] and SPECT imaging clearly visualized tumor tissues *in vivo*. It should be emphasized that *in vivo* imaging of MT1-MMP relevant to the malignancy of tumors was achieved in this study.

Radiolabeled antibodies typically have a low rate of blood clearance, which can be a crucial pitfall for radioimmunodetection and radioimmunotherapy. To solve this problem, antibody fragments (Fab, scFv) and engineered variants (diabodies, triabodies, minibodies) have been investigated.[21] However, these techniques can cause problems such as reduced immunoreactivity of antibody derivatives and reduced delivery of radioactivity to the targeted organs.[22] On the other hand, the pre-targeting method has been investigated extensively, especially in tumor treatment, because of the selective accumulation of radioactivity to the targeted organ without a loss of antibody immunoreactivity and the high S/N ratio that can be achieved during the first hours after administration.[9] In fact, the introduction of a few biotins did not affect the immunoreactivity, and sulfo-NHS-LC-biotin with a spacer arm of 22.4 Å was used to minimize the steric effect by streptavidin. Recently, other reports have also shown that a pre-targeting method was effective for *in vivo* imaging of biofunctional molecules such as CD20.[11] Therefore, the pre-targeting method seems to address many of the limitations of the direct radioimaging agent approach.

In this paper, accumulated radioactivity in the tumor and T/B ratios were significantly higher in the true pre-targeting study than in the negative control pre-targeting study (ANOVA test). Thus, the accumulation of radioactivity in tumors pre-targeted with anti-MT1-MMP mAb-SAv suggests that specificity for MT1-MMP is responsible for this effect. Moreover, the tumor accumulation of ^{125}I-IBB in the absence of pre-targeting was not observed, which suggests the tumor accumulation of ^{125}I-IBB in the pre-targeting study depended on the pre-targeting antibody. As a result of rapid clearance of ^{125}I-IBB, the pre-targeting method achieved high T/B ratios significantly earlier than did our previously studied directly labeled anti-MT1-MMP mAb.[8] The T/B ratio obtained within 1 h with the pre-targeting method was higher than that from the directly labeled anti-MT1-MMP mAb at 48 h. Furthermore, tumor to lung and tumor to heart ratios from the pre-targeting method were 10.6 and 4.5 fold higher compared with the directly labeled anti-MT1-MMP mAb at 1 h after the injection of the radiolabeled probe. These results indicate the pre-targeting method provides clearer imaging of MT1-MMP in breast tumors during the first hours after administration.

Specific accumulation for MT1-MMP can be estimated by comparing the radioactivity in the tumor and T/B ratios in the true pre-targeting method with those in the negative control method. About 30—40% specific accumulation was achieved in this study, although ^{125}I-IBB accumulated in the tumor to some extent in the negative control pre-targeting study unexpectedly. This is probably caused in part by passive accumulation of the streptavidinylated antibody as a macromolecule, that is enhanced permeability and retention effect.[23] In addition, an RYD sequence contained in SAv,[24] homologous to the RGD domain, might interact with integrins expressed on the cell surface of tumors.[25] By replacing SAv with neutravidin, which lacks the RYD domain, a more specific imaging of MT1-MMP may be achieved in the future.

In the SPECT imaging study of the pre-targeting method, tumors were clearly visualized. High levels of radioactivity were also observed in the kidneys and intestine. This may be due to the high kidney uptake of pre-targeted streptavidinylated anti-MT1-MMP mAb that is dependent on the biodistribution of streptavidin itself[26] and to physiological ^{125}I-IBB accumulation in the intestine. ^{125}I-IBB also accumulated in the bladder because its molecular weight leads to glomeruli filtration. It should be stressed that chest organs such as the lungs and heart, and the liver were not visualized, which indicates the potential of this method for adequate imaging of breast tumors expressing MT1-MMP. In addition, preliminary Western blotting analysis using lysates from human breast cancer cells (MDA-MB-231) detected a high level of human MT1-MMP expression,[8] suggesting that this method may be useful in a clinical setting. We are currently investigating the effectiveness of this pre-targeting method across a variety of tumor cells that differently express MT1-MMP.

In this study, $^{123/125}$I-labeled biotin was used to demonstrate the availability of pre-targeting method for MT1-MMP because its stability, affinity to avidin and biodistribution was well examined.[19] On the other hand, ^{99m}Tc generated by a ^{99}Mo/^{99m}Tc generator on site at any time on demand is attractive for clinical use, and ^{99m}Tc-biotin may also deserve investigation on pre-targeting methods.

Biodistribution of streptavidinylated anti-MT1-MMP antibody was examined for 1—72 h. T/B ratios increased in a time dependent manner and were highest at 72 h, which has the potential that T/B ratios may be improved at the later stage after injection, leading the high contrast images of MT1-MMP. On the other hand, sensitivity can be dependent on the absolute radioactivity of $^{123/125}$I-IBB in the tumor tissue, which is an important indicator on molecular imaging. In this study, accumulation of streptavidinylated antibody in the tumor was decreased with time, indicating that $^{123/125}$I-IBB was also predicted to show the lower tumor uptake at the later stage. Thus, by taking into consideration radioactivity in the tumor and T/B ratios, we adopted the protocol such that radiolabeled biotin was administered 72 h after pre-treatment with streptavidinylated antibodies, although further studies are needed for setting the optimal interval. To date, some reports have shown that clearing agents (*e.g.* galactosylated biotin–albumin conjugate) can readily (a few hours) remove excess streptavidinylated antibodies in the circulation *via* the liver without loss of biotin binding sites in the tumor,[27,28] thus leading to a shortening of the interval needed between administration of the streptavidinylated antibody and radiolabeled biotin. In this study, we obtained the data that accumulation of streptavidinylated anti-MT1-MMP mAb was reduced after the peak at 24 h post-injection probably because of the internalization and metabolism in the tumor cells.[29] Thus, the clearing agents may enable the administration of radiolabeled biotin at the earlier time point when streptavidinylated antibody in the tumor is highly retained. This strategy will help establish an optimal protocol for sensitive MT1-MMP imaging with an aim toward clinical application.

CONCLUSION

The results clearly demonstrate the effectiveness of the pre-targeting method for imaging MT1-MMP in breast tumors with greater sensitivity and earlier post-injection analysis in comparison with the direct-radiolabeled antibody. As

mentioned previously, the amino acid sequence of the MT1-MMP protein is highly conserved among species including mouse, rat, rabbit, and human; our results obtained in experiments using rodents and MT1-MMP probes may provide important information for clinical applications and may prove to be beneficial in the diagnosis of breast tumor malignancy in the clinical setting.

Acknowledgments This study was supported by Grants-in-Aid for Scientific Research and by the 21st Century Center of Excellence Programs at Kyoto University "Knowledge Information Infrastructure for Genome Science" from the Ministry of Education, Culture, Sports, Science and Technology, Japan. A portion of this study was conducted in conjunction with the project, "R&D of Molecular Imaging Equipment for Malignant Tumor Therapy Support," which was supported by the New Energy and Industrial Technology Development Organization (NEDO), Japan.

REFERENCES

1) Sato H., Takino T., Okada Y., Cao J., Shinagawa A., Yamamoto E., Seiki M., *Nature* (London), **370**, 61—65 (1994).
2) Deryugina E. I., Quigley J. P., *Cancer Metastasis Rev.*, **25**, 9—34 (2006).
3) Jones J. L., Glynn P., Walker R. A., *J. Pathol.*, **189**, 161—168 (1999).
4) Knauper V., Bailey L., Worley J. R., Soloway P., Patterson M. L., Murphy G., *FEBS Lett.*, **532**, 127—130 (2002).
5) Holmbeck K., Bianco P., Caterina J., Yamada S., Kromer M., Kuznetsov S. A., Mankani M., Robey P. G., Poole A. R., Pidoux I., Ward J. M., Birkedal-Hansen H., *Cell*, **99**, 81—92 (1999).
6) Zhou Z., Apte S. S., Soininen R., Cao R., Baaklini G. Y., Rauser R. W., Wang J., Cao Y., Tryggvason K., *Proc. Natl. Acad. Sci. U.S.A.*, **97**, 4052—4057 (2000).
7) Chen P. S., Zhai W. R., Zhou X. M., Zhang J. S., Zhang Y. E., Ling Y. Q., Gu Y. H., *World J. Gastroenterol.*, **7**, 647—651 (2001).
8) Temma T., Sano K., Kuge Y., Kamihashi J., Takai N., Ogawa Y., Saji H., *Biol. Pharm. Bull.*, **32**, 1272—1277 (2009).
9) Boerman O. C., van Schaijk F. G., Oyen W. J., Corstens F. H., *J. Nucl. Med.*, **44**, 400—411 (2003).
10) Kraeber-Bodere F., Rousseau C., Bodet-Milin C., Ferrer L., Faivre-Chauvet A., Campion L., Vuillez J. P., Devillers A., Chang C. H., Goldenberg D. M., Chatal J. F., Barbet J., *J. Nucl. Med.*, **47**, 247—255 (2006).
11) Goldenberg D. M., Sharkey R. M., Paganelli G., Barbet J., Chatal J. F., *J. Clin. Oncol.*, **24**, 823—834 (2006).
12) Goldenberg D. M., Rossi E. A., Sharkey R. M., McBride W. J., Chang C. H., *J. Nucl. Med.*, **49**, 158—163 (2008).
13) Green N. M., *Methods Enzymol.*, **184**, 51—67 (1990).
14) Jemal A., Siegel R., Ward E., Murray T., Xu J., Smigal C., Thun M. J., *CA Cancer J. Clin.*, **56**, 106—130 (2006).
15) Zhang Y., Wang C., Zhang Y., Sun M., *Biochem. Biophys. Res. Commun.*, **325**, 1240—1245 (2004).
16) Sato T., del Carmen Ovejero M., Hou P., Heegaard A. M., Kumegawa M., Foged N. T., Delaisse J. M., *J. Cell Sci.*, **110**, 589—596 (1997).
17) Kinoh H., Sato H., Tsunezuka Y., Takino T., Kawashima A., Okada Y., Seiki M., *J. Cell Sci.*, **109**, 953—959 (1996).
18) Ishino S., Mukai T., Kuge Y., Kume N., Ogawa M., Takai N., Kamihashi J., Shiomi M., Minami M., Kita T., Saji H., *J. Nucl. Med.*, **49**, 1677—1685 (2008).
19) Foulon C. F., Alston K. L., Zalutsky M. R., *Bioconj. Chem.*, **8**, 179—186 (1997).
20) Zalutsky M. R., Narula A. S., *Int. J. Rad. Appl. Instrum. A*, **38**, 1051—1055 (1987).
21) Behr T. M., Becker W. S., Bair H. J., Klein M. W., Stuhler C. M., Cidlinsky K. P., Wittekind C. W., Scheele J. R., Wolf F. G., *J. Nucl. Med.*, **36**, 430—441 (1995).
22) Holliger P., Hudson P. J., *Nat. Biotechnol.*, **23**, 1126—1136 (2005).
23) Iyer A. K., Khaled G., Fang J., Maeda H., *Drug Discov. Today*, **11**, 812—818 (2006).
24) Argarana C. E., Kuntz I. D., Birken S., Axel R., Cantor C. R., *Nucl. Acids Res.*, **14**, 1871—1882 (1986).
25) Ruoslahti E., Pierschbacher M. D., *Science*, **238**, 491—497 (1987).
26) Schechter B., Arnon R., Colas C., Burakova T., Wilchek M., *Kidney Int.*, **47**, 1327—1335 (1995).
27) Pantelias A., Pagel J. M., Hedin N., Saganic L., Wilbur S., Hamlin D. K., Wilbur D. S., Lin Y., Stone D., Axworthy D., Gopal A. K., Press O. W., *Blood*, **109**, 4980—4987 (2007).
28) Sharkey R. M., Karacay H., Griffiths G. L., Behr T. M., Blumenthal R. D., Mattes M. J., Hansen H. J., Goldenberg D. M., *Bioconj. Chem.*, **8**, 595—604 (1997).
29) Wang X., Ma D., Keski-Oja J., Pei D., *J. Biol. Chem.*, **279**, 9331—9336 (2004).

MOLECULAR IMAGING AND BIOLOGY

Mol Imaging Biol (2010)
DOI: 10.1007/s11307-010-0463-1

RESEARCH ARTICLE

A Pre-targeting Strategy for MR Imaging of Functional Molecules Using Dendritic Gd-Based Contrast Agents

Kohei Sano,[1] Takashi Temma,[1] Takashi Azuma,[2] Ryusuke Nakai,[2] Michiko Narazaki,[3] Yuji Kuge,[1,4] Hideo Saji[1]

[1]*Department of Patho-Functional Bioanalysis, Graduate School of Pharmaceutical Sciences, Kyoto University, 46-29 Yoshida Shimoadachi-cho, Sakyo-ku, Kyoto, 606-8501, Japan*

[2]*Department of Medical Simulation Engineering Research Center for Nano Medical Engineering Institute for Frontier Medical Sciences, Kyoto University, Kyoto, 606-8501, Japan*

[3]*Department of Systems Science, Graduate School of Informatics, Kyoto University, Kyoto, 606-8501, Japan*

[4]*Central Institute of Isotope Science, Hokkaido University, Sapporo, 060-8638, Japan*

Abstract

Purpose: We aimed to establish a magnetic resonance imaging (MRI) protocol for the sensitive and specific imaging of functional molecules with a pre-targeting strategy utilizing the streptavidin–biotin interaction. Membrane type-1 matrix metalloproteinase (MT1-MMP) was selected as the target molecule.

Procedures: The biotinylated polyamidoamine dendrimer (PAMAM)-based contrast agent (Bt-PAMAM-DTPA(Gd)) was prepared, and its proton relaxivity ($r1$) and affinity to streptavidin were evaluated. Tumor-bearing mice were pre-targeted with streptavidin-conjugated anti-MT1-MMP monoclonal antibody (mAb), streptavidin-conjugated negative control IgG, or saline and 3 days later were injected with Bt-PAMAM-DTPA(Gd) followed immediately by MRI for a period of 3 h.

Results: High $r1$ (15.5 L $mmol^{-1}$ s^{-1}) and 1.9-fold higher affinity than D-biotin were obtained. Significantly higher relative tumor signals were observed in mice pre-targeted with streptavidin-conjugated anti-MT1-MMP mAb (165% at 3 h *vs.* pre-administration) than with saline or streptavidin-conjugated negative control IgG ($P<0.0001$).

Conclusions: This pre-targeting approach can accomplish sensitive and specific *in vivo* MRI of functional molecules.

Key words: Pre-targeting, Polyamidoamine dendrimer (PAMAM), Membrane type-1 matrix metalloproteinase, Magnetic resonance imaging

Introduction

Magnetic resonance imaging (MRI), characterized by a remarkable spatial resolution, is a powerful tool for noninvasive morphologic diagnosis of diseases including cancer. Recently, the application of MRI to functional molecular imaging coupled with anatomical information has been explored. To realize functional molecular imaging by MRI, contrast agents are required that possess a high relaxation to produce high MR signals to compensate for the low intrinsic sensitivity of MRI [1] in addition to selectively accumulating in the targeting site.

Gadolinium (Gd) chelates conjugated to macromolecules such as liposomes, micelles, and dendrimers can give rise to enhanced proton relaxivities in comparison with simple,

Correspondence to: Hideo Saji; *e-mail:* hsaji@pharm.kyoto-u.ac.jp

Published online: 08 December 2010

small molecule contrast agents such as Gd-diethylenetriamine pentaacetic acid (Gd-DTPA) [2–4]. This effect is due to a restriction in thermal flexibility leading to increased interactions between the Gd atom and surrounding water molecules [5–7]. Some groups have developed monoclonal antibody (mAb)-conjugated macromolecular contrast agents for imaging integrin αvβ3 or human epidermal growth factor receptor type 2 (HER2) in tumors, which successfully increased the tumor signal intensity by 15–30% [8, 9]. However, many researchers have failed to demonstrate *in vivo* functional molecular imaging using macromolecules conjugated with several Gd chelates and targeting moieties like antibodies and peptides because the pharmacokinetics of the targeting moieties was significantly altered by the introduction of macromolecular contrast agents, which resulted in low target recognition and high accumulation of the labeling agent in non-targeted tissues [10, 11]. Furthermore, when antibody-conjugated macromolecular contrast agents are injected at a Gd dose (0.1 mmol Gd/kg) necessary for adequate imaging, excess antibodies (on the order of milligrams per mouse) are typically administered, which leads to major limitations of cost and *in vivo* toxicity.

Thus, in this study, to overcome these problems and to realize functional molecular MRI by a macromolecule-based contrast agent, we aimed to use a pre-targeting strategy that utilizes the high affinity interaction between streptavidin and biotin ($Kd=10^{-15}$ M) [12]. In this pre-targeting method, the first step is to administer a streptavidin-conjugated target-specific antibody. In the second step, after selective accumulation of streptavidin-conjugated antibody in the targeted tissue and clearance of unbound targeting agent from the circulation, a biotin-bound imaging probe is injected. As the post-administration contrast agent, polyamidoamine dendrimer (PAMAM) was selected as the base structure since it is structurally well-defined and functional moieties including biotins and Gd chelates for both targeting and signal emission functions can easily be attached to the large number of its surface amino groups. The pre-targeting strategy is expected to provide selective and effective accumulation of the PAMAM-based contrast agent to the targeted site and a high S/N ratio during the first hours following administration, as has been observed in radioimmunotherapy and radioimmunodetection [13–16], and to potentially lead to lower *in vivo* toxicity [17, 18].

Thus, in this paper, we describe our efforts to establish a sensitive and specific *in vivo* MRI protocol for imaging functional molecules utilizing a pre-targeting strategy that combines a streptavidin-conjugated antibody with a PAMAM-based contrast agent modified with biotins. As the targeted biomolecule, membrane type-1 matrix metalloproteinase (MT1-MMP) was selected. Since MT1-MMP is exclusively expressed in tumors and is closely associated with metastasis [19] and invasion [20], MT1-MMP is a potential imaging target for evaluating tumor malignancy.

Materials and Methods

Synthesis of Streptavidin-Conjugated Anti-MT1-MMP mAb

Streptavidin-conjugated anti-MT1-MMP mAb and streptavidin-conjugated negative control IgG were synthesized according to a previously described method [14]. Briefly, EZ-Link® sulfosuccinimidyl-6-(biotinamido) hexanoate (sulfo-NHS-LC-biotin; Pierce, Inc.) was added to a solution of anti-MT1-MMP mAb (113-5B7, Daiichi Fine Chemical Co.) in a molar ratio of 12:1. The mixture was gently stirred for 30 min at room temperature and then was purified with a diafiltration membrane (Amicon Ultra 4 (MWCO 30,000), Millipore Co.). A solution of biotinylated anti-MT1-MMP mAb was added to a solution of streptavidin (SAv; Pierce, Inc.) in a 1:3 molar ratio. The mixture was incubated for 1 h at 37°C followed by purification twice by affinity chromatography using a HiTrap rProtein A column (GE Healthcare Bioscience). The eluate containing anti-MT1-MMP mAb-SAv was concentrated with a diafiltration membrane (MWCO 30,000), and the protein concentration was determined by the bicinchoninate (BCA) method. The purification was monitored by a size exclusion chromatograph using a 300×4.6-mm i.d. TSK-Gel Super SW 3000 column (Tosoh Co., Japan) eluted with phosphate buffer (0.1 M, pH 6.8) at a flow rate of 0.1 mL/min. Comparison of molecular mass standards (Oriental Yeast Co., Japan) of the absorbance at 280 nm indicated that a peak at 30.3 min was consistent with the presence of a 210-kDa streptavidin-conjugated anti-MT1-MMP mAb. Furthermore, streptavidin-conjugated anti-MT1-MMP mAb retained 81.3% of the anti-MT1-MMP mAb immunoreactivity, which was confirmed by flow cytometry.

Synthesis of Bt-PAMAM-DTPA(Gd)

EZ-Link® sulfo-NHS-LC-biotin was added to a solution of PAMAM (generation 4 (G4)) (Sigma Aldrich) in a molar ratio of 20:1. The mixture was stirred for 30 min at room temperature and then was applied to a diafiltration membrane (MWCO 10,000) to remove unbound biotins as well as to change the buffer to phosphate buffer (0.1 M, pH 9.0). After purification, the incorporation ratio of biotins conjugated to each dendrimer was measured using an EZ™ Biotin Quantitation Kit (Pierce, Inc.). The biotinylated PAMAM was reacted with a 64-fold molar excess of 2-(*p*-isothiocyanatobenzyl)-diethylenetriamine pentaacetic acid (*p*-SCN-Bz-DTPA) (Macrocyclics) at 40°C for 24 h. During the reaction, the pH was maintained at 9.0 with 1 N NaOH. An additional equal amount of *p*-SCN-Bz-DTPA was added after 24 h, and the reaction was incubated for another 24 h at 40°C. The resulting preparation was purified by diafiltration membrane (MWCO 10,000). After purification, the number of DTPAs incorporated into each G4 dendrimer was checked by chelate titration using $ZnSO_4$ (indicator: 4-(2-pyridylazo)resorcinol, NH_3/NH_4^+, pH 10), according to a previously described method with some modification [21]. Purified Bt-PAMAM-DTPA was mixed with $GdCl_3$ (Sigma Aldrich) in citrate buffer (0.3 M, pH 5.0) for 2 h at 40°C. The excess Gd was removed by diafiltration membrane (MWCO 10,000) while simultaneously changing the buffer to PBS (0.1 M, pH 7.4). The number of Gd incorporated into the dendrimer was checked by separating the free Gd and Bt-PAMAM-DTPA

(Gd) with a diafiltration filter after labeling the Bt-PAMAM-DTPA with ^{153}Gd and nonradioactive Gd. For comparison purposes, PAMAM-DTPA(Gd) containing one biotin (Bt_1-PAMAM-DTPA (Gd)) was also prepared in a similar manner.

Stability of Bt-PAMAM-DTPA(Gd) in Mouse Plasma

^{153}Gd-labeled Bt-PAMAM-DTPA(Gd) was prepared by reacting Bt-PAMAM-DTPA(Gd) with ^{153}Gd (1 μCi, PerkinElmer Japan Co., Osaka, Japan) and non-radioactive Gd in 0.3 M citrate buffer at pH 5.0 for 2 h at 40°C. ^{153}Gd-labeled Bt-PAMAM-DTPA(Gd) (30 μL) was added to mouse plasma collected from female C3H/He mice (270 μL), and the plasma samples were incubated at 37°C for 0, 3, and 24 h. After incubation, aliquots of the samples were drawn, and radioactivity was analyzed by size-exclusion chromatography with a PD-10 column (GE Healthcare Bioscience) using saline as eluent.

Affinity of Bt-PAMAM-DTPA(Gd) for Streptavidin

Competition assays of ^{125}I-(3-iodobenzoyl)norbiotinamide (^{125}I-IBB), a radiolabeled biotin derivative synthesized as reported previously [22], were performed by incubating streptavidin (Pierce, Inc.; 400 μL, 2 μg/mL), ^{125}I-IBB (50 μL, 5 μCi), and various concentrations of Bt-PAMAM-DTPA(Gd), Bt_1-PAMAM-DTPA(Gd), and D-biotin (Nacalai Tesque, Kyoto, Japan; 50 μL, 10^{-8}~10^{-4} M) in PBS (0.1 M, pH 7.4) for 60 min at 37°C. At the end of the incubation, the mixture was applied to a size exclusion column with a Sephadex G-50 Fine (GE Healthcare Bioscience), followed by measurement of the radioactivity from the column eluent (containing macromolecules) with a NaI well-type scintillation counter (1470WIZARD, PerkinElmer Japan Co.). Nonspecific binding was determined in the presence of 10 mg/mL D-biotin. The 50% inhibitory concentrations (IC_{50}s) were determined from displacement curves of the percent inhibition of ^{125}I-IBB binding *vs.* the inhibitor concentration.

Preparation of Tumor-Bearing Animals

Female C3H/He mice (5 weeks old), supplied by Japan SLC Co. (Hamamatsu, Japan), were housed under a 12-h light/12-h dark cycle and were given free access to food and water. The animal experiments in this study were conducted in accordance with institutional guidelines and were approved by the Kyoto University Animal Care Committee, Japan.

FM3A mouse breast carcinoma cells were supplied by the Health Science Research Resources Bank (Osaka, Japan). They were cultured in DMEM medium (Nissui Pharmaceutical Co.) supplemented with 10% fetal bovine serum at 37°C in a humidified atmosphere containing 5% CO_2 and 95% air and had a 10.6-h doubling time.

FM3A cells were suspended in 0.01 M PBS (pH 7.4) followed by subcutaneous inoculation into the right hind leg of the mouse (5×10^6 cells/100 μL/mouse) [23]. The tumor volume was estimated by (length)×(width)^2/2 [24] over a 10-day tumor growth period. The average size of the tumors was 213±82 mm^3 on the MRI study day. The expression of MT1-MMP in FM3A cells and tumor tissues was confirmed by western blotting and immunohistochemistry [25].

Magnetic Resonance Imaging

MRI was performed using a clinical 1.5 Tesla MR scanner (MAGNETOM Symphony Sonata, Siemens). All T_1-weighted MR images were acquired with a multislice spin-echo pulse sequence. MRI data were analyzed using the ImageJ software.

Phantom Study

Solutions of Gd-DTPA (Sigma Aldrich) and Bt-PAMAM-DTPA (Gd) were prepared with a Gd concentration in the range of 10 to 500 μM in vials with an inner diameter of 15 mm followed by the MR scan using a knee coil (20.5 cm in diameter) at 20°C. To obtain proton relaxivity ($r1$) for samples, spin-echo images were obtained using a sequence with TR=500, 1,000, 1,500, and 2,000 ms and with TE=15 ms. The imaging parameters were as follows: field-of-view, 256×128 mm; matrix, 256×128; slice thickness, 7 mm; and number of average, 3.

In Vivo Study

Mice (n=4) bearing FM3A tumors in the right thigh received streptavidin-conjugated anti-MT1-MMP mAb (50 μg/100 μL in saline) via tail vein. Three days later, Bt-PAMAM-DTPA(Gd) (0.1 mmol Gd/kg, 100 μL in PBS (0.1 M, pH 7.4), i.v.) was injected followed by data acquisition by MRI at several time points over a 3-h post-injection period under sodium pentobarbital (50 mg/kg, i.p.) anesthesia. All MR images were obtained using a hand-made round surface coil (5.5 cm in diameter) fixed by a custom constructed coil holder. The imaging parameters were as follows: TR/TE, 300/5.2 ms; field-of-view, 128×96 mm; matrix, 256×192; slice thickness, 1.5 mm; and number of average, 3. MRI studies were also conducted as above on FM3A tumor-bearing mice (n=3) pre-treated with saline (100 μL) or streptavidin-conjugated negative control IgG (50 μg/100 μL in saline). The signal intensity was calculated by drawing a region of interest around the tumor, muscle in the contralateral hind limb, and kidneys. The relative signal intensity in each tissue was defined as the signal intensity after administration of Bt-PAMAM-DTPA(Gd) divided by the signal intensity before administration.

Statistical Analysis

Unpaired Student's t test was used to evaluate the significance of differences of $r1$ between Bt-PAMAM-DTPA(Gd) and Gd-DTPA. To compare the time courses of relative signal intensity in the tumor and kidneys and tumor/muscle (T/M) signal ratios among Bt-PAMAM-DTPA(Gd) pre-targeted by streptavidin-conjugated anti-MT1-MMP mAb, streptavidin-conjugated negative control IgG, and saline, two-way repeated measures ANOVA with post-hoc analysis by the Tukey–Kramer test was

performed. Differences at the 95% confidence level ($P<0.05$) were considered significant.

Results

Characterization of Bt-PAMAM-DTPA(Gd)

Bt-PAMAM-DTPA(Gd) was synthesized in four steps from PAMAM in a yield of 63%. PAMAM was conjugated to 9.9± 1.3 biotins and 43.6±1.9 DTPAs, which were quantitatively coordinated to Gd. Bt_1-PAMAM-DTPA(Gd) containing 1.0± 0.1 biotin and 47.6±2.2 DTPAs on PAMAM dendrimer was also synthesized. The ^{153}Gd-labeled Bt-PAMAM-DTPA(Gd), which was incubated with mouse plasma for 24 h, did not release any low molecular weight metabolites or free radiometals (Fig. 1).

The competitive binding assay revealed that all of the contrast agents inhibited the binding of ^{125}I-IBB to streptavidin in a dose-dependent manner (Fig. 2). The IC_{50}s for Bt-PAMAM-DTPA(Gd), Bt_1-PAMAM-DTPA(Gd), and D-biotin were 32±31, 1,390±1,220, and 60±45 nM, respectively, demonstrating that Bt-PAMAM-DTPA(Gd) had about 1.9- and 43.2-fold higher affinity to streptavidin than D-biotin and Bt_1-PAMAM-DTPA(Gd).

MR Imaging Study (Phantom Study)

The *in vitro* T_1-weighted MR images with Bt-PAMAM-DTPA(Gd) and Gd-DTPA are shown in Fig. 3a. Water and PBS were used as baselines. With the same Gd concentration, the signals with Bt-PAMAM-DTPA(Gd) were higher compared to Gd-DTPA. The longitudinal relaxation rate ($1/T_1$) *vs.* the concentration of Gd for both contrast agents are shown in Fig. 3b with good linear fits (R^2=1.00 and 0.99 for Bt-PAMAM-DTPA(Gd) and Gd-DTPA, respectively). Calculated $r1$ values (L mmol^{-1} s^{-1}) for Bt-PAMAM-DTPA(Gd) and Gd-DTPA were 15.5±1.1 and 3.6± 0.1, respectively, which shows that the proton relaxivity of Bt-PAMAM-DTPA(Gd) was 4.3-fold higher than that of Gd-DTPA ($P<0.0001$).

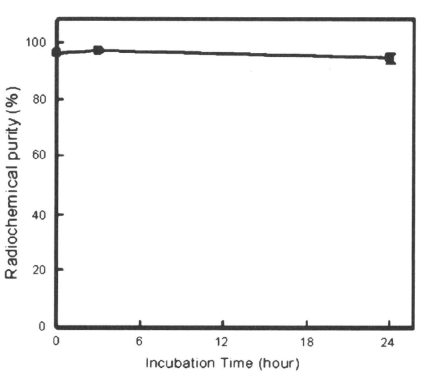

Fig. 1. Size exclusion analysis of ^{153}Gd-labeled Bt-PAMAM-DTPA(Gd) radioactivity after incubation at 37°C in mouse plasma. The *error bars* represent standard deviations.

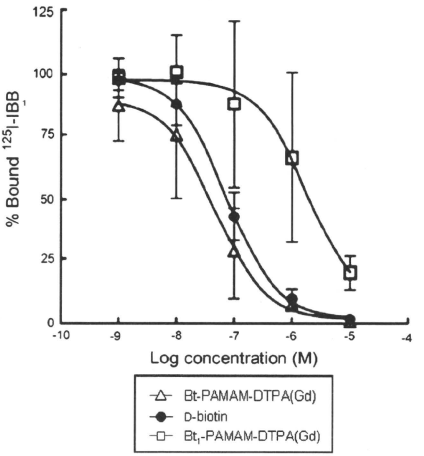

Fig. 2. Inhibition of ^{125}I-IBB binding to streptavidin by D-biotin, Bt-PAMAM-DTPA(Gd), or Bt_1-PAMAM-DTPA(Gd).

MR Imaging Study (In Vivo Study)

Fig. 4a (coronal) and b (transaxial) show *in vivo* T_1-weighted MR images of tumor-bearing mice before and at 5 and 180 min after injection of Bt-PAMAM-DTPA(Gd) following pre-treatment with streptavidin-conjugated anti-MT1-MMP mAb (MT1-MMP), streptavidin-conjugated negative control IgG (negative control), or saline (saline). In the MT1-MMP group, the most intense signal was observed in the margin of the tumor, as compared with the tumor core, over the 180-min period. The relative signal intensity (rSI) in the tumor and the relative T/M ratio were strongly enhanced just after administration of Bt-PAMAM-DTPA(Gd) and were highly maintained for 3 h after the contrast agent injection which displayed rapid clearance from the circulation (Fig. 4c, d). These signals were significantly greater than those from the negative control group ($P<0.05$ (at 44 and 55 min), $P<0.01$ (at 2 and 3 h)). In the saline group, Bt-PAMAM-DTPA(Gd) readily disappeared from the circulation and mainly accumulated in the kidneys. Though the relative signal intensity in the tumor also increased

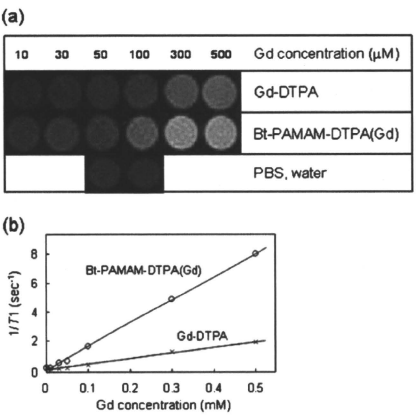

Fig. 3. **a** *In vitro* T_1-weighted MR measurements of different concentrations of Gd (micromolar) from Gd-DTPA and Bt-PAMAM-DTPA(Gd) in PBS at 1.5 T. PBS and water were used as references. These images show that at all concentrations, the signals are greater for Bt-PAMAM-DTPA(Gd) than for Gd-DTPA. **b** Longitudinal relaxation rate ($1/T_1$) *vs.* the concentration of Gd from Gd-DTPA (*crosses*) and Bt-PAMAM-DTPA (Gd) (*circles*) in PBS at 1.5 T are presented with good linear fits (R^2>0.99). The $r1$ value for Bt-PAMAM-DTPA(Gd) was 4.3-fold higher than for Gd-DTPA.

(190%) just after administration of Bt-PAMAM-DTPA(Gd), it decreased to the basal level (115%) within 3 h (Fig. 4c). A slightly higher tumor signal was obtained in the negative control group than in the saline group only 3 h after injection of Bt-PAMAM-DTPA(Gd) (P<0.01). The time-dependent change of relative T/M ratios was similar to that of the relative signal intensity in the tumor (Fig. 4d). The time-dependent change of relative signal intensity in the kidneys was very similar in all three groups (Fig. 4e).

Discussion

In this study, we accomplished visualization of MT1-MMP by MRI using a pre-targeting method with a PAMAM-based contrast agent (Bt-PAMAM-DTPA(Gd)) which possesses high proton relaxivity and high affinity to streptavidin. For future applications, this pre-targeting method based on the interaction between biotin and streptavidin is promising for the detection of functional molecules, such as biomarkers in tumors like MT1-MMP, by *in vivo* MRI.

Although several macromolecular contrast agents have been developed for functional molecular imaging with MRI using a mAb or peptide as the targeting moiety, these attempts have been largely unsuccessful because the macromolecular contrast agents, such as an antibody attached to a dendrimer, have a poorer targeting ability and slower pharmacokinetics in the circulation than the targeting moiety alone, which leads to an inadequately low S/N ratio for several days post-injection [10, 11]. Thus, we focused on a pre-targeting strategy whose effectiveness in elevating the S/N ratio shortly after injection has been well documented in the field of radioimmunotherapy [13, 26]. In the pre-targeting strategy, high affinity between the pre- and post-administered agents is required; thus, the affinity of a post-administered biotinylated contrast agent to streptavidin needed to be evaluated. In this study, Bt-PAMAM-DTPA (Gd) containing approximately ten biotins in the structure showed 43.2- and 1.9-fold higher affinity to streptavidin compared with Bt_1-PAMAM-DTPA(Gd) containing only one biotin per dendrimer and D-biotin, respectively, which suggests a multivalent effect for Bt-PAMAM-DTPA(Gd) binding to streptavidin. Zhu *et al.* recently reported the MRI of functional molecules by a pre-targeting approach [27]; however, the authors failed to show a significant tumor image probably because of the small number of biotins per dendrimer (~4 biotins per dendrimer). Therefore, in a pre-targeting method where a macromolecule is used as the post-administered agent, it is essential that an optimal number of biotins on the macromolecule be evaluated.

In the streptavidin-conjugated anti-MT1-MMP mAb-treated group, MR signals in the tumor and T/M ratios were highly maintained following Bt-PAMAM-DTPA(Gd) administration compared with the saline-treated group, which suggests that the tumor accumulation of Bt-PAMAM-DTPA(Gd) depended on the pre-targeted streptavidin-conjugated anti-MT1-MMP mAb. Furthermore, MR signals in the tumor and T/M ratios were also significantly higher in the streptavidin-conjugated anti-MT1-MMP mAb-treated group than those in the negative control, which suggests that the accumulation of Bt-PAMAM-DTPA(Gd) was primarily specific for MT1-MMP. The slightly significant difference in relative tumor signals for the negative control and saline groups is probably caused in part by passive accumulation of the pre-targeted streptavidin-conjugated antibody as a macromolecule due to an enhanced permeability and retention effect [28].

Previously, to determine the optimal interval between injections of streptavidin-conjugated anti-MT1-MMP mAb and Bt-PAMAM-DTPA(Gd), the biodistribution of ^{125}I-labeled streptavidin-conjugated anti-MT1-MMP mAb was evaluated in C3H/He mice bearing FM3A mouse breast carcinoma [14]. From consideration of the high accumulation of streptavidin-conjugated antibody in the tumor and the high tumor-to-blood ratio at 72 h, we adopted this time as the interval between pre- and post-administrations in this study. Recently, some reports have shown that clearing agents (e.g., galactosylated biotin-albumin conjugate) can readily (within a few hours) clear surplus streptavidin-conjugated antibody from the circulation to the liver where the complex is metabolized and excreted without the loss of biotin binding sites in the tumor [29–31], thereby shortening

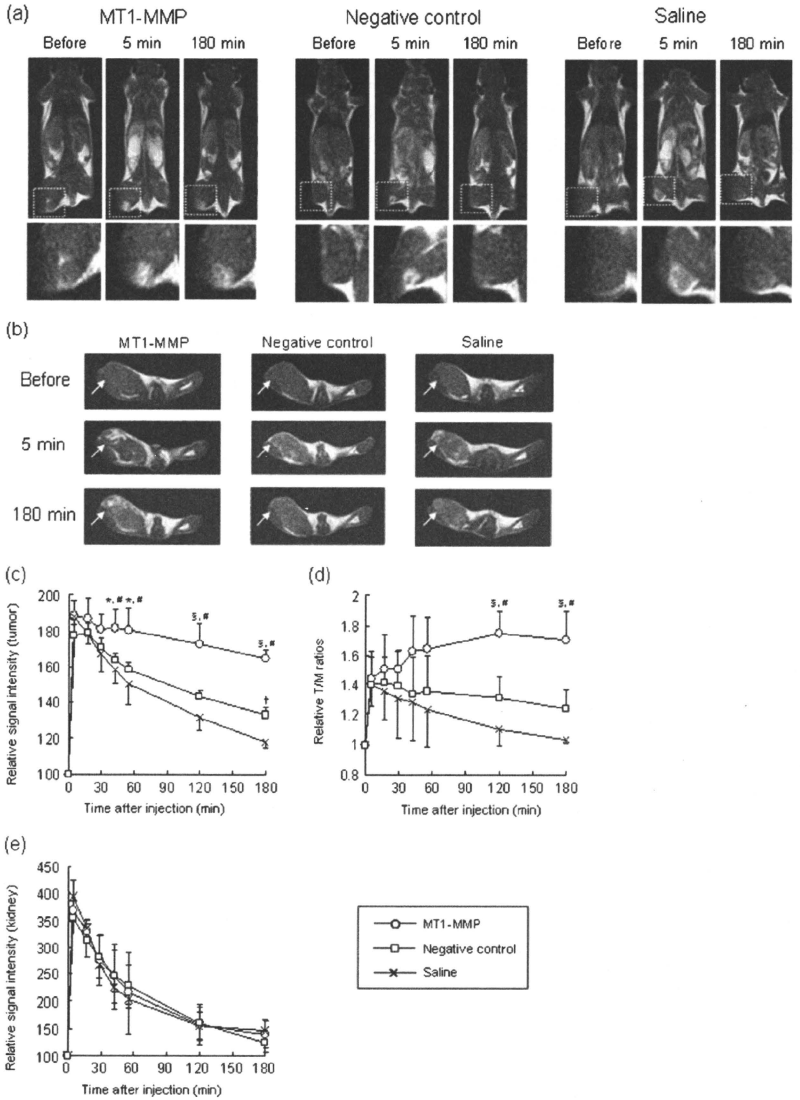
(a)
MT1-MMP
Negative control
Saline
Before
5 min
180 min
(b)
MT1-MMP
Negative control
Saline
Before
5 min
180 min
(c)
Relative signal intensity (tumor)
Time after injection (min)
(d)
Relative T/M ratios
Time after injection (min)
(e)
Relative signal intensity (kidney)
Time after injection (min)
MT1-MMP
Negative control
Saline

◀ **Fig. 4. a, b** *In vivo* T_1-weighted MR images of C3H/He mice before and at 5 and 180 min after injection of Bt-PAMAM-DTPA(Gd) following pre-treatment with streptavidin-conjugated anti-MT1-MMP mAb (*MT1-MMP*), streptavidin-conjugated negative control IgG (*Negative control*), or saline (*Saline*). The coronal (**a**) and transaxial (**b**) images are shown. *Arrows* or *dotted squares* indicate the tumor site. Enlarged images of the *dotted square* regions are also shown. **c–e** The dynamic change of signal intensity in the tumor by Bt-PAMAM-DTPA(Gd) (**c**) and relative tumor to muscle ratios (**d**) following pre-treatment with streptavidin-conjugated anti-MT1-MMP mAb (*MT1-MMP*, *circles*), streptavidin-conjugated negative control IgG (*Negative control*, *squares*), or saline (*Saline*, *crosses*). **e** The dynamic change of signal intensity in the kidney for each animal group. *$P<0.05$; §$P<0.01$ *vs. Negative control*; #$P<0.01$ *vs. Saline*; †$P<0.01$ *Negative control vs. Saline*.

the interval between injections. In the future, by taking advantage of this type of strategy, we can establish an optimal protocol for MT1-MMP imaging for clinical applications.

Dendrimers are a class of highly branched spherical polymers, with a variety of properties, such as chemical structure, size, molecular weight, and functional groups that can be easily manipulated at the molecular level through their synthesis. The pharmacokinetics of the dendrimer is susceptible to control with its generation number such that it may be highly bioavailable, an important consideration for a variety of applications, especially in the biomedical field [32]. Here, PAMAM dendrimer was chosen as the base structure of the contrast agent for post-administration. PAMAM dendrimer (G4) with an ethylene diamine core has a molecular weight of 14,215 Da and possesses 64 amino groups on the surface of the molecule [33]. In this study, 10 biotins and 44 Gds for specific targeting and sensitive imaging were introduced onto the dendrimer. An *in vitro* MR study showed that the relaxivity of Bt-PAMAM-DTPA(Gd) was 4.3-fold higher than Gd-DTPA, which indicates the effectiveness of Bt-PAMAM-DTPA(Gd) as a contrast agent with high proton relaxivity as expected because of slow tumbling rates and a short water residence time [2, 5].

The post-administered contrast agent in a pre-targeting study should satisfy the following two requirements besides specific affinity to pre-administered streptavidin: rapid blood clearance and low nonspecific accumulation in the tumor. It has been reported that a PAMAM (G4) dendrimer is quickly excreted via glomerular filtration primarily during the first pass (the blood α phase half-life, 2.5 min; β phase half-life, 35 min [34]), and not via the bile pathway. In addition, these dendrimers exhibit no measurable leakage from normal blood vessels because of their moderate size (ca. 6 nm) [2, 34–37], which leads to low nonspecific accumulation in the tumor caused by passive accumulation based on an enhanced permeability and retention effect. PAMAM (G4)-based MR contrast agents can be effective as imaging probes, as supported by the experimental data that showed low MR signals observed in the tumors of the saline pre-targeted group while intense signals were observed in the kidneys after the acute disappearance of Bt-PAMAM-DTPA (Gd) from the circulation.

As mentioned above, in the case of antibody-conjugated dendrimer-based contrast agents, excess antibodies (on the order of milligrams per mouse) are typically administered when injected at a Gd dose (0.1 mmol Gd/kg) necessary for adequate imaging, which leads to major limitations of cost and toxicity. On the other hand, our pre-targeting strategy could control the amount of injected streptavidin-conjugated antibody by corresponding to the targeted molecule (about 50 μg per mouse for MT1-MMP), which would be useful for reducing the cost and toxicity of the imaging process.

In the application of dendrimers *in vivo*, cytotoxicity is often a major issue. To date, as has been widely demonstrated for other polycations, dendrimers bearing amino termini display concentration- and commonly generation-dependent cytotoxicity [38] and potent hemolytic activity [39]. These effects could be attributable to the electrostatic interactions of the positively charged dendrimer with the negatively charged cell membrane under physiological pH. Nevertheless, Bt-PAMAM-DTPA(Gd) used in this study was negatively charged due to modifications of the amino termini to bind biotin and DTPA such that it could be acceptable *in vivo*. This assertion is supported by a report that PAMAM dendrimers bearing carboxylate termini display dramatically lower toxicity to cells [40]. We also plan to acetylate or succinylate the free amino groups to further reduce the positive charge of the complexes if needed to decrease toxicity and hemolytic activity. The rapid excretion of Bt-PAMAM-DTPA(Gd) via glomerular filtration should alleviate adverse effects such as nephrogenic systemic fibrosis [41] derived from released Gd, as compared with macromolecular contrast agents which have slow elimination pharmacokinetics [11, 42], although further analysis of the cytotoxicity is needed.

Conclusions

The pre-targeting method utilizing the specific interaction between streptavidin and biotin enabled the visualization of MT1-MMP expressing tumors by 1.5 T MRI with high S/N ratios during the first hours following administration of a contrast agent, Bt-PAMAM-DTPA(Gd). The results suggest that this method may be beneficial to diagnosing tumor malignancy in a clinical setting. In future work, this method could be applied to the imaging of a variety of pathologic functional molecules expressed on cell surfaces.

Acknowledgments. This study was supported by Grants-in-Aid for Scientific Research and by the 21st Century Center of Excellence Programs at Kyoto University "Knowledge Information Infrastructure for Genome Science" from the Ministry of Education, Culture, Sports, Science and Technology, Japan. A part of this study was conducted as a part of the project "R&D of Molecular Imaging Equipment for Malignant Tumor Therapy Support," supported by the New Energy and Industrial Technology Development Organization (NEDO), Japan.

Conflicts of Interest. The authors have no conflict of interest.

References

1. Caravan P (2006) Strategies for increasing the sensitivity of gadolinium based MRI contrast agents. Chem Soc Rev 35:512–523
2. Kobayashi H, Brechbiel MW (2003) Dendrimer-based macromolecular MRI contrast agents: characteristics and application. Mol Imaging 2:1–10
3. Accardo A, Tesauro D, Roscigno P et al (2004) Physicochemical properties of mixed micellar aggregates containing CCK peptides and Gd complexes designed as tumor specific contrast agents in MRI. J Am Chem Soc 126:3097–3107
4. Mulder WJ, Strijkers GJ, van Tilborg GA, Griffioen AW, Nicolay K (2006) Lipid-based nanoparticles for contrast-enhanced MRI and molecular imaging. NMR Biomed 19:142–164
5. Nicolle GM, Toth E, Schmitt-Willich H, Raduchel B, Merbach AE (2002) The impact of rigidity and water exchange on the relaxivity of a dendritic MRI contrast agent. Chemistry 8:1040–1048
6. Toth EE, Vauthey S, Pubanz D, Merbach AE (1996) Water exchange and rotational dynamics of the dimeric gadolinium(III) complex [BO{Gd(DO3A)(H(2)O)}(2)]: a variable-temperature and -pressure (17)O NMR study(1). Inorg Chem 35:3375–3379
7. Toth E, Merbach AE (1998) Water exchange dynamics: the key for high relaxivity contrast agents in medical magnetic resonance imaging. ACH - Models Chem 135:873–884
8. Sipkins DA, Cheresh DA, Kazemi MR et al (1998) Detection of tumor angiogenesis *in vivo* by alphaVbeta3-targeted magnetic resonance imaging. Nat Med 4:623–626
9. Lee JH, Huh YM, Jun YW et al (2007) Artificially engineered magnetic nanoparticles for ultra-sensitive molecular imaging. Nat Med 13:95–99
10. Boswell CA, Eck PK, Regino CA et al (2008) Synthesis, characterization, and biological evaluation of integrin alphavbeta3-targeted PAMAM dendrimers. Mol Pharm 5:527–539
11. Kobayashi H, Sato N, Saga T et al (2000) Monoclonal antibody-dendrimer conjugates enable radiolabeling of antibody with markedly high specific activity with minimal loss of immunoreactivity. Eur J Nucl Med 27:1334–1339
12. Green NM (1990) Avidin and streptavidin. Meth Enzymol 184:51–67
13. Boerman OC, van Schaijk FG, Oyen WJ, Corstens FH (2003) Pretargeted radioimmunotherapy of cancer: progress step by step. J Nucl Med 44:400–411
14. Sano K, Temma T, Kuge Y et al (2010) Radioimmunodetection of MT1-MMP relevant to tumor malignancy with pre-targeting method. Biol Pharm Bull 32:1589–1595
15. Axworthy DB, Reno JM, Hylarides MD et al (2000) Cure of human carcinoma xenografts by a single dose of pretargeted yttrium-90 with negligible toxicity. Proc Natl Acad Sci USA 97:1802–1807
16. Paganelli G, Malcovati M, Fazio F (1991) Monoclonal antibody pretargetting techniques for tumour localization: the avidin-biotin system. International Workshop on Techniques for Amplification of Tumour Targetting. Nucl Med Commun 12:211–234
17. Goldenberg DM, Sharkey RM, Paganelli G, Barbet J, Chatal JF (2006) Antibody pretargeting advances cancer radioimmunodetection and radioimmunotherapy. J Clin Oncol 24:823–834
18. Sharkey RM, Karacay H, Cardillo TM et al (2005) Improving the delivery of radionuclides for imaging and therapy of cancer using pretargeting methods. Clin Cancer Res 11:7109s–7121s
19. Deryugina EI, Quigley JP (2006) Matrix metalloproteinases and tumor metastasis. Cancer Metastasis Rev 25:9–34
20. Shiomi T, Okada Y (2003) MT1-MMP and MMP-7 in invasion and metastasis of human cancers. Cancer Metastasis Rev 22:145–152
21. Laus S, Sour A, Ruloff R, Toth E, Merbach AE (2005) Rotational dynamics account for pH-dependent relaxivities of PAMAM dendrimeric, Gd-based potential MRI contrast agents. Chemistry 11:3064–3076
22. Foulon CF, Alston KL, Zalutsky MR (1997) Synthesis and preliminary biological evaluation of (3-iodobenzoyl)norbiotinamide and ((5-iodo-3-pyridinyl)carbonyl)norbiotinamide: two radioiodinated biotin conjugates with improved stability. Bioconjug Chem 8:179–186
23. Kudo T, Ueda M, Kuge Y et al (2009) Imaging of HIF-1-active tumor hypoxia using a protein effectively delivered to and specifically stabilized in HIF-1-active tumor cells. J Nucl Med 50:942–949
24. Zhang Y, Wang C, Zhang Y, Sun M (2004) C6 glioma cells retrovirally engineered to express IL-18 and Fas exert FasL-dependent cytotoxicity against glioma formation. Biochem Biophys Res Commun 325:1240–1245
25. Temma T, Sano K, Kuge Y et al (2009) Achievement of MT1-MMP imaging shortly after radioligand administration by pretargeting strategy with SPECT. J Nucl Med 50(suppl):337P
26. Kraeber-Bodere F, Rousseau C, Bodet-Milin C et al (2006) Targeting, toxicity, and efficacy of 2-step, pretargeted radioimmunotherapy using a chimeric bispecific antibody and 131I-labeled bivalent hapten in a phase I optimization clinical trial. J Nucl Med 47:247–255
27. Zhu W, Okollie B, Bhujwalla ZM, Artemov D (2008) PAMAM dendrimer-based contrast agents for MR imaging of Her-2/neu receptors by a three-step pretargeting approach. Magn Reson Med 59:679–685
28. Iyer AK, Khaled G, Fang J, Maeda H (2006) Exploiting the enhanced permeability and retention effect for tumor targeting. Drug Discov Today 11:812–818
29. Pantelias A, Pagel JM, Hedin N et al (2007) Comparative biodistributions of pretargeted radioimmunoconjugates targeting CD20, CD22, and DR molecules on human B-cell lymphomas. Blood 109:4980–4987
30. Sharkey RM, Karacay H, Griffiths GL et al (1997) Development of a streptavidin-anti-carcinoembryonic antigen antibody, radiolabeled biotin pretargeting method for radioimmunotherapy of colorectal cancer. Studies in a human colon cancer xenograft model. Bioconjug Chem 8:595–604
31. Lin Y, Pagel JM, Axworthy D et al (2006) A genetically engineered anti-CD45 single-chain antibody-streptavidin fusion protein for pretargeted radioimmunotherapy of hematologic malignancies. Cancer Res 66:3884–3892
32. Tomalia DA, Reyna LA, Svenson S (2007) Dendrimers as multi-purpose nanodevices for oncology drug delivery and diagnostic imaging. Biochem Soc Trans 35:61–67
33. Tomalia DA, Naylor AM, Goddard WA (1990) Starburst dendrimers: molecular-level control of size, shape, surface chemistry, topology, and flexibility from atoms to macroscopic matter. Angew Chem Int Ed Engl 29:138–175
34. Kobayashi H, Sato N, Hiraga A et al (2001) 3D-micro-MR angiography of mice using macromolecular MR contrast agents with polyamidoamine dendrimer core with reference to their pharmacokinetic properties. Magn Reson Med 45:454–460
35. Sato N, Kobayashi H, Hiraga A et al (2001) Pharmacokinetics and enhancement patterns of macromolecular MR contrast agents with various sizes of polyamidoamine dendrimer cores. Magn Reson Med 46:1169–1173
36. Choyke PL, Kobayashi H (2006) Functional magnetic resonance imaging of the kidney using macromolecular contrast agents. Abdom Imaging 31:224–231
37. Kobayashi H, Brechbiel MW (2005) Nano-sized MRI contrast agents with dendrimer cores. Adv Drug Deliv Rev 57:2271–2286
38. Roberts JC, Bhalgat MK, Zera RT (1996) Preliminary biological evaluation of polyamidoamine (PAMAM) starburst dendrimers. J Biomed Mater Res 30:53–65
39. Malik N, Wiwattanapatapee R, Klopsch R et al (2000) Dendrimers: relationship between structure and biocompatibility *in vitro*, and preliminary studies on the biodistribution of 125I-labelled polyamidoamine dendrimers *in vivo*. J Control Release 65:133–148
40. Jevprasesphant R, Penny J, Jalal R et al (2003) The influence of surface modification on the cytotoxicity of PAMAM dendrimers. Int J Pharm 252:263–266
41. Buhaescu I, Izzedine H (2008) Gadolinium-induced nephrotoxicity. Int J Clin Pract 62:1113–1118
42. Kobayashi H, Kawamoto S, Jo SK et al (2003) Macromolecular MRI contrast agents with small dendrimers: pharmacokinetic differences between sizes and cores. Bioconjug Chem 14:388–394

Eur J Nucl Med Mol Imaging (2010) 37:2093–2104
DOI 10.1007/s00259-010-1521-2

ORIGINAL ARTICLE

Imaging with radiolabelled anti-membrane type 1 matrix metalloproteinase (MT1-MMP) antibody: potentials for characterizing atherosclerotic plaques

Yuji Kuge · Nozomi Takai · Yuki Ogawa · Takashi Temma · Yan Zhao · Kantaro Nishigori · Seigo Ishino · Junko Kamihashi · Yasushi Kiyono · Masashi Shiomi · Hideo Saji

Received: 17 December 2009 / Accepted: 3 June 2010 / Published online: 13 July 2010

Abstract
Purpose Membrane type 1 matrix metalloproteinase (MT1-MMP) activates pro-MMP-2 and pro-MMP-13 to their active forms and plays important roles in the destabilization of atherosclerotic plaques. This study sought to determine the usefulness of ^{99m}Tc-labelled monoclonal antibody (mAb), recognizing MT1-MMP, for imaging atherosclerosis in a rabbit model (WHHLMI rabbits).
Methods Anti-MT1-MMP monoclonal IgG_3 and negative control IgG_3 were radiolabelled with ^{99m}Tc after derivatization with 6-hydrazinonicotinic acid (HYNIC) to yield ^{99m}Tc-MT1-MMP mAb and ^{99m}Tc-IgG_3, respectively. WHHLMI and control rabbits were injected with these radio-probes. The aorta was removed and radioactivity was measured at 24 h after the injection. Autoradiography and histological studies were performed.
Results ^{99m}Tc-MT1-MMP mAb accumulation in WHHLMI rabbit aortas was 5.4-fold higher than that of control rabbits. Regional ^{99m}Tc-MT1-MMP mAb accumulation was positively correlated with MT1-MMP expression (r=0.59, p<0.0001), while ^{99m}Tc-IgG_3 accumulation was independent of MT1-MMP expression (r=0.03, p=NS). The highest ^{99m}Tc-MT1-MMP mAb accumulation was found in atheromatous lesions (4.8±1.9, %ID×BW/mm^2×10^2), followed in decreasing order by fibroatheromatous (1.8±1.3), collagen-rich (1.6±1.0) and neointimal lesions (1.5±1.5). In contrast, ^{99m}Tc-IgG_3 accumulation was almost independent of the histological grade of lesions.
Conclusion Higher ^{99m}Tc-MT1-MMP mAb accumulation in grade IV atheroma was shown in comparison with neointimal lesions or other more stable lesions. Nuclear imaging with ^{99m}Tc-MT1-MMP mAb, in combination with CT and MRI, could provide new diagnostic imaging capabilities for detecting vulnerable plaques, although further investigations to improve target to blood ratios are strongly required.

Keywords Atherosclerosis · Imaging · Matrix metalloproteinase · Antibody · Rabbit

Y. Kuge · N. Takai · Y. Ogawa · T. Temma · K. Nishigori · S. Ishino · J. Kamihashi · Y. Kiyono · H. Saji
Department of Patho-functional Bioanalysis,
Graduate School of Pharmaceutical Sciences, Kyoto University,
Kyoto, Japan

Y. Kuge · Y. Zhao
Department of Tracer Kinetics & Bioanalysis,
Graduate School of Medicine, Hokkaido University,
Sapporo, Japan

Y. Kuge (✉)
Central Institute of Isotope Science, Hokkaido University,
Kita 15 Nishi 7, Kita-ku,
Sapporo 060-0815, Japan
e-mail: kuge@ric.hokudai.ac.jp

Y. Kiyono
Biomedical Imaging Research Center, University of Fukui,
Fukui, Japan

M. Shiomi
Institute for Experimental Animals,
Kobe University Graduate School of Medicine,
Kobe, Japan

Introduction

Since the rupture of atherosclerotic plaques and subsequent thrombus formation are the major causes of ischaemic diseases, such as cerebral and myocardial infarctions [1–3],

the detection of atherosclerotic plaques at higher risk for rupture is clinically important for early selection and administration of appropriate therapy. There are several techniques for imaging atherosclerotic plaques, such as computed tomography (CT), magnetic resonance imaging (MRI), ultrasound (US) and intravascular ultrasound (IVUS). These non-invasive anatomical imaging modalities offer excellent resolution and visualize the arterial lumen or calcifications. These modalities can identify the morphological alteration of atherosclerotic plaque and play important roles in finding the patients whose lesion vulnerability needs to be further evaluated. To date, however, there are no non-invasive diagnostic tools available for routine clinical use to accurately characterize atherosclerotic plaques at higher risk of rupture. Accordingly, the development of such non-invasive tools is urgently required. Using specific radio-probes, it may be possible for nuclear imaging to characterize atherosclerotic plaques as quantitative images based on cellular and biological changes, which surpasses morphological information and may help selectively detect atherosclerotic plaques at higher risk of rupture [4, 5]. Thus, the development of radio-probes is of great concern in the clinical diagnosis of atherosclerosis.

Plaques that are prone to rupture are morphologically characterized by a thin fibrous cap overlying a large lipid core. Matrix metalloproteinases (MMPs) degrade extracellular matrix that constitutes the fibrous cap of the plaques, resulting in destabilization of atherosclerotic plaques [6–8]. Increased expression of MMP-2 and MMP-9 has been demonstrated within human atherosclerotic lesions and critically implicated in plaque rupture [7, 9, 10]. MMP-2 and MMP-9 are known to cleave native type IV, V, VII and X collagens and elastin, as well as the degradation products of collagens types I, II and III after proteolysis by collagenases, such as MMP-1 and MMP-13. Thus, MMPs are considered to be involved in plaque instability [8] and are potential targets for diagnostic imaging of atherosclerotic plaques at higher risk of rupture [11, 12]. MMPs can be divided into two groups: soluble MMPs and membrane-bound MMPs. Most soluble MMPs, including MMP-2 and MMP-9, are released from cells as zymogens and require extracellular post-translational cleavage to gain biological activity [8, 13]. A membrane-bound MMP, membrane type 1 matrix metalloproteinase (MT1-MMP or MMP-14), mediates activation of pro-MMP-2 to active MMP-2 and pro-MMP-13 to active MMP-13 on the cell surface [13–15]. In our recent animal study, co-distribution of MT1-MMP and MMP-2 was demonstrated in grade IV atheroma, indicating a possible role for MT1-MMP in destabilization of atherosclerotic plaques [16]. Expression of MT1-MMP has also been found within human atherosclerotic plaques [17, 18]. Accordingly, MT1-MMP may be an important determinant of destabilization of atherosclerotic plaques and detection of MT1-MMP expression may be useful for the assessment of atherosclerotic plaques.

Taken together, nuclear imaging of MT1-MMP could provide molecular and cellular information concerning the destabilization of atherosclerotic plaques. Thus, we designed and prepared ^{99m}Tc-labelled anti-MT1-MMP monoclonal IgG (^{99m}Tc-MT1-MMP mAb) as a radio-probe for imaging atherosclerosis. Using an atherosclerosis model (myocardial infarction-prone Watanabe heritable hyperlipidaemic rabbits, WHHLMI rabbits) [19], we investigated accumulation of ^{99m}Tc-MT1-MMP mAb in atherosclerotic lesions in comparison with histological characteristics. From the data, the potential of ^{99m}Tc-MT1-MMP mAb for imaging atherosclerosis was evaluated.

Materials and methods

Design and preparation of ^{99m}Tc-MT1-MMP mAb

A purified mouse monoclonal antibody (mAb) to an oligopeptide (residues 319 to 333, numbered from the signal peptide) on human MT1-MMP (113-5B7, mouse IgG3, Daiichi Fine Chemical Co., Ltd., Toyama, Japan) [14] was used. For the control study, negative control mouse IgG_3 (ab18392, Abcam, Cambridge, UK) was used.

The anti-MT1-MMP monoclonal IgG_3 (MT1-MMP mAb) and negative control IgG_3 (IgG_3) were radiolabelled with ^{99m}Tc (^{99m}Tc-MT1-MMP mAb and ^{99m}Tc-IgG_3, respectively) after derivatization with 6-hydrazinonicotinic acid (HYNIC), according to the procedures reported previously [20–22] with slight modifications. Briefly, HYNIC-*N*-hydroxysuccinimide (NHS) was reacted with MT1-MMP mAb and IgG_3 to obtain precursors for radiolabelling (HYNIC-MT1-MMP mAb and HYNIC-IgG_3, respectively) and then purified by diafiltration. HYNIC-NHS (25 μl, 5 mg/ml) in dry *N*,*N*-dimethylformamide (DMF) was added to MT1-MMP mAb and IgG_3 solutions in 0.15 M borate buffer (pH 8.5, 2 mg/400 μl), respectively. After gentle stirring with protection from light for 2 h at room temperature, size-exclusion (SE) filtration with a diafiltration membrane [Amicon Ultra-4 (MWCO 30,000), Millipore Co., Billerica, MA, USA] using 0.01 M citrate buffer (pH 5.2) was performed to remove aggregated protein and to obtain HYNIC-MT1-MMP mAb and HYNIC-IgG_3. The purified HYNIC-MT1-MMP mAb and HYNIC-IgG_3 were stored at 4°C and used for the subsequent radiolabelling.

Radiolabelling was performed just before each experiment. To the purified HYNIC-MT1-MMP mAb and HYNIC-IgG_3 solutions (300 μg/500 μl), an equal volume of [^{99m}Tc](tricine)$_2$, prepared by the method of Larsen et al. [23], was added to obtain ^{99m}Tc-MT1-MMP mAb and